SERDP

FINAL REPORT

Thermal-Enhanced Photochemical and Alkaline Destruction of PFAS in Sorbent Regenerants and Membrane Concentrates

Jinyong Liu
University of California, Riverside

January 2025

SERDP Project ER21-1117

REPORT DOCUMENTATION PAGE

Form Approved
OMB No. 0704-0188

1. REPORT DATE *(DD-MM-YYYY)*	**2. REPORT TYPE**	**3. DATES COVERED** *(From - To)*
10/01/2025	SERDP Final Report	9/30/2021 - 9/29/2024

4. TITLE AND SUBTITLE

Thermal-Enhanced Photochemical and Alkaline Destruction of PFAS in Sorbent Regenerants and Membrane Concentrates

5a. CONTRACT NUMBER
21-P-0116

5b. GRANT NUMBER

5c. PROGRAM ELEMENT NUMBER

6. AUTHOR(S)
Jinyong Liu
University of California, Riverside

5d. PROJECT NUMBER
ER21-1117

5e. TASK NUMBER

5f. WORK UNIT NUMBER

7. PERFORMING ORGANIZATION NAME(S) AND ADDRESS(ES)
University of California, Riverside
Department of Chemical and Environmental Engineering
900 University Ave
UC Riverside, Bourns Hall B321
Riverside, CA 92521

8. PERFORMING ORGANIZATION REPORT NUMBER
ER21-1117

9. SPONSORING/MONITORING AGENCY NAME(S) AND ADDRESS(ES)
Office of the Deputy Assistant Secretary of Defense (Energy Resilience & Optimization)
3500 Defense Pentagon, RM 5C646
Washington, DC 20301-3500

10. SPONSOR/MONITOR'S ACRONYM(S)
SERDP

11. SPONSOR/MONITOR'S REPORT NUMBER(S)
ER21-1117

12. DISTRIBUTION/AVAILABILITY STATEMENT
DISTRIBUTION STATEMENT A. Approved for public release: distribution unlimited.

13. SUPPLEMENTARY NOTES

14. ABSTRACT
UV/sulfite treatment has demonstrated excellent performance and low consumption of chemicals and energy. Previously, most photochemical treatment studies were conducted at 20°C using cooling water, but the heat generated by UV lamps could raise the water temperature and potentially accelerate the reaction and enhance the defluorination. Besides photochemical redox transformations, spontaneous defluorination from specific H-containing polyfluorinated structures in alkaline conditions could occur. Such reactions could be potentially enhanced at elevated temperatures (below 100 °C) and higher pH. However, the temperature effects on PFAS degradation and underlying mechanisms were unknown. Therefore, specific objectives of this project include (1) achieving deeper PFAS defluorination by the thermal-enhanced UV/sulfite treatment; (2) achieving defluorination of UV-recalcitrant PFAS structures by thermal-enhanced alkaline treatment; and (3) minimizing the energy consumption through the thermal enhancement.

15. SUBJECT TERMS
Per- and polyfluoroalkyl substance (PFAS); perfluorocarboxylate (PFCA); perfluoroether sulfonate (PFSA); fluorotelomer carboxylate (FTCA); ultra-violet (UV) lamp; thermal energy; elevated temperature; hydrated electron; quantum yield; sulfite; iodide; acceleration; degradation; defluorination; transformation product (TP); reaction mechanism; hydroxide ion; HF elimination; double bond

16. SECURITY CLASSIFICATION OF:			**17. LIMITATION OF ABSTRACT**	**18. NUMBER OF PAGES**	**19a. NAME OF RESPONSIBLE PERSON**
a. REPORT	**b. ABSTRACT**	**c. THIS PAGE**			Jinyong Liu
UNCLASS	UNCLASS	UNCLASS	UNCLASS	57	**19b. TELEPHONE NUMBER** *(Include area code)* 951-827-1481

Table of Contents

List of Tables

List of Figures

List of Acronyms

BDE: **b**ond **d**issociation **e**nergy
deF%: defluorination percentage
DI: **de**i**o**nized
EE/O: **e**lectrical **e**nergy consumed by one **o**rder of magnitude decay of the pollutant
ESTCP: **E**nvironmental **S**ecurity **T**echnology **C**ertification **P**rogram
FTCA: **f**luoro**t**elomer **c**a*rbo*nic **a**cid
FTSA: **f**luoro**t**elomer **s**ulfonic **a**cid
FTUCA: **f**luoro**t**elomer **u**nsaturated **c**arbonic **a**cid
HF: **h**ydrogen **f**luoride
HRMS: **h**igh **r**esolution **m**ass **s**pectrometry
IC: **i**on **c**hromatography
ISE: **i**on-**s**elective **e**lectrode
LC-MS: **l**iquid **c**hromatography-**m**ass **s**pectrometry
PFAS: **p**er- and poly**f**luoro**a**lkyl **s**ubstance
PFBA: **p**er**f**luoro**b**utanoic **a**cid
PFBS: **p**er**f**luoro**b**utane **s**ulfonic acid
PFCA: **p**er**f**luoro **c**arboxylic **a**cid
PFHxS: **p**er**f**luoro**he**x**a**ne **s**ulfonic acid
PFOA: **p**er**f**luoro**o**ctanoic **a**cid
PFOS: **p**er**f**luoro**o**ctane **s**ulfonic acid
PFPrA: **p**er**f**luoro**pr**opionic **a**cid
PFSA: **p**er**f**luoro **s**ulfonic **a**cid
PI: **p**rincipal **i**nvestigator
SERDP: **S**trategic **E**nvironmental **R**esearch and **D**evelopment **P**rogram
TFA: **t**ri**f**luoro**a**cetate
TISAB: **t**otal **i**onic **s**trength **a**djustment **b**uffer
TP: **t**ransformation **p**roduct
UCR: **U**niversity of **C**alifornia, **R**iverside
UHPLC: **u**ltra-**h**igh-**p**erformance **l**iquid **c**hromatography
UV: **u**ltra-**v**iolet

Keywords

Per- and polyfluoroalkyl substance (PFAS); perfluorocarboxylate (PFCA); perfluoroether sulfonate (PFSA); fluorotelomer carboxylate (FTCA); ultra-violet (UV) lamp; thermal energy; elevated temperature; hydrated electron; quantum yield; sulfite; iodide; acceleration; degradation; defluorination; transformation product (TP); reaction mechanism; hydroxide ion; HF elimination; double bond

Acknowledgments

This report represents the results and conclusions from Dr. Jinyu Gao (Tasks 1 and 3), and Dr. Dandan Rao (Task 2). Early-stage development for preliminary results was contributed by Dr. Zekun Liu under the support by SERDP ER18-1289. The project team thanks Dr. Andrea Leeson and the support staff from the SERDP office for their help and guidance.

Abstract

Introduction and Objectives

UV/sulfite treatment has demonstrated excellent performance and low consumption of chemicals and energy. Previously, most photochemical treatment studies were conducted at 20°C using cooling water, but the heat generated by UV lamps could raise the water temperature and potentially accelerate the reaction and enhance the defluorination. Besides photochemical redox transformations, spontaneous defluorination from specific H-containing polyfluorinated structures in alkaline conditions could occur. Such reactions could be potentially enhanced at elevated temperatures (below 100 °C) and higher pH. However, the temperature effects on PFAS degradation and underlying mechanisms were unknown. Therefore, specific objectives of this project include (1) achieving deeper PFAS defluorination by the thermal-enhanced UV/sulfite treatment; (2) achieving defluorination of UV-recalcitrant PFAS structures by thermal-enhanced alkaline treatment; and (3) minimizing the energy consumption through the thermal enhancement.

Technical Approach

PFAS destruction by UV/sulfite was conducted in 2 L photochemical reactors with one or more low-pressure mercury UV lamps at variable temperatures. PFAS destruction by heated alkaline treatment was conducted in glass beakers on a heating plate. The PFAS degradation performance was evaluated by the rate and extent of parent compound decay and fluoride ion release. Transformation products were analyzed with high-resolution mass spectrometry. Model compounds were used to probe/verify the proposed reaction mechanisms.

Results

The highest rates of PFAS decay and defluorination were achieved at 50°C. This temperature allowed the cleavage of relatively strong C–F bonds difficult at 20°C. FFurther raising the temperature up to 90°C resulted in adverse effects. Photochemical measurements suggested that the elevated temperature lowered the quantum yield of hydrated electrons. The competition between accelerated elemental reaction steps versus decreased quantum yield of hydrated electrons resulted in the maximum rate for the overall reaction at 50°C. The addition of iodide for reaction acceleration also benefited from the elevated temperature. The heat dissipated from the UV lamps alone could provide sufficient enhancement in the rate and extent of PFAS defluorination. A series of H-containing PFAS allowed non-redox defluorination. Elevated temperature (up to 90ºC) and pH (up to 14) not only accelerated the reaction rate but also intensified the level of defluorination via additional mechanisms, many of which remain elusive. Because of the structure specificity, just heating the water at pH 12 after UV/sulfite treatment cannot replace oxidation treatment to achieve 100% defluorination for a majority of legacy PFAS.

Benefits

This project confirms the positive effect of thermal energy, which is the dominant way of electrical energy dissipation from UV lamps. The findings have been applied to pilot-scale reactions to treat real samples. Scientifically, the findings provide critical insights into the photochemical generation of hydrated electrons at varying temperatures. The study on alkaline non-redox defluorination also provides novel insights into the additional PFAS degradation mechanisms under heated alkaline conditions (e.g., UV/sulfite at pH 12 without temperature control). In addition, the results caution analytical researchers on sample preservation to avoid gradual defluorination from pollutants and transformation products in alkaline solutions.

Executive Summary

Introduction and Objectives

Among the recently developed PFAS degradation technologies that can work at ambient temperature and pressure, the UV/sulfite system stands out for its excellent performance and low consumption of chemicals and energy. UV/sulfite generates hydrated electrons (e_{aq}^-) that can effectively cleave C–F bonds in PFAS. Previously, the PI's lab and many other labs maintained the temperature of UV/sulfite treatment at 20°C or lower using a cooling jacket to simulate typical ambient conditions in natural waters. In the absence of the cooling jacket, however, the heat generated by the UV lamp could raise the water temperature, potentially expediting the reaction and improving the defluorination percentage. When this project was proposed in early 2020, the treatment performance and underlying mechanism regarding temperature effects on PFAS degradation under the UV/sulfite system were unknown.

We also anticipated that adjusting the number of UV lamps will expedite PFAS defluorination not only because of the irradiation intensity but also due to the temperature change by heat dissipation from UV lamps. When the project was proposed, it was unclear whether adding more UV lamps and removing the cooling system could help cleave additional C–F bonds toward a higher overall defluorination percentage. Adding more UV lamps entails higher energy consumption, and it was unclear whether this approach could proportionally enhance the rate or extent of PFAS defluorination.

During early explorations, the PI's lab also observed spontaneous defluorination from specific H-containing polyfluorinated structures at pH 12. The defluorination became faster in the presence of elevated temperature (below the water boiling point of 100 °C) and alkaline conditions (pH 9–14, without UV/sulfite treatment). Under the same conditions, the corresponding fully fluorinated structures showed no reactivity. This phenomenon prompted us to consider that H atoms in polyfluorinated structures might initiate new defluorination mechanisms independent of redox processes and C−F bond dissociation energies.

With the knowledge gaps presented above, for this project, we primarily aimed to elucidate the reaction mechanisms underlying the thermal enhancement of PFAS degradation, with (Task 1) or without (Task 2) UV/sulfite treatment, and to further optimize energy efficiency by determining the optimal reaction temperature and the number of UV lamps (Task 3).

Objectives

The overall objectives of this limited-scope project are to obtain a comprehensive understanding and determine key parameters for the thermal-enhanced reductive and alkaline destruction of PFAS. The direct technical goal is to use a limited amount of thermal energy (i.e., heating the water up to 90°C) to enhance the treatment effectiveness and energy efficiency for PFAS degradation. The outcomes validate the "thermal-enhanced" treatment strategy and will benefit the management of PFAS-enriched waste streams in practical demonstration projects.

Three specific objectives were:

(i) Achieve deep or near-complete defluorination from a majority of PFAS structures by the thermal-enhanced single-step UV/sulfite treatment; if not successful, elucidate the effect of temperature and the reaction mechanisms.

(ii) Achieve rapid decay and deep defluorination of recalcitrant PFAS structures such as short-chain sulfonic acids and fluorotelomers by thermal-enhanced photochemical and alkaline treatment; if not successful, elucidate the structure-reactivity relationship and the reaction mechanism.

(iii) Minimize the consumption of both electricity and chemicals through the thermal-enhanced treatment strategy.

Through this project, we collected a comprehensive set of performance data and advanced the engineering aspects of UV/sulfite technology toward field demonstration operations (ESTCP ER21-5152). We elucidated detailed mechanisms for thermal-enhanced PFAS degradation regarding (1) the optimal temperature at 50°C rather than 90°C, (2) the key photochemical parameters that determine the reaction rate, and (3) the role of hydroxide and structure-reactivity relationship in non-photochemical alkaline defluorination. The findings provide novel perceptions of thermal energy effects in the photochemical system.

Technical Approach

The technical approaches include the following experiments (see the main body for details):

- Preparation of stock solutions of PFAS and reaction chemicals.
- Photochemical reactor design and setup.
- PFAS degradation and transformation product analysis with LC-HRMS.
- Measurement of fluoride ion release.
- Quantification of short-chain PFCAs and sulfite with IC.

Results and Discussion

The results are presented in three Sections in the main body of the Final Report:

4.1 Thermal-enhanced UV/sulfite defluorination
4.2 Thermal-enhanced alkaline defluorination
4.3 Further optimization of energy efficiency

The **first highlight of this project** is the systematic investigation of the effect of temperature on PFAS degradation under UV/sulfite treatment. The highest rates of PFAS decay and defluorination are achieved at 50°C (Figure E1 and Table E1). For the three major PFAS structure families (PFCAs, PFSAs, and FTCAs), the decay rates increased by 21–85% when the solution temperature was raised from 20 to 50°C. For the recalcitrant structures that could not be effectively degraded by UV/sulfite treatment (e.g., n=4 PFBS and 4:3 FTCA), the percentage of decay was also improved by 9–19% after 24 h. The defluorination percentage also increased by 3–22% (particularly significant for recalcitrant PFAS structures). The TP analysis suggested that the reaction at 50°C also allowed the cleavage of relatively strong C–F bonds.

In contrast, further raising the temperature to 90°C resulted in adverse effects. Compared to 20°C, the rates of PFAS decay decreased by 41–66% at 90°C. The percentages of decay and defluorination were similar to those at 20°C, but the rates were slower. Photochemical measurements suggested that the elevated temperature lowered the quantum yield of hydrated electrons. The competition between accelerated elemental reaction steps versus decreased quantum

yield of hydrated electrons resulted in the maximum rate for the overall reaction at 50°C. Further increasing the temperature to up to 90°C resulted in a gradual slowing down of the overall reaction.

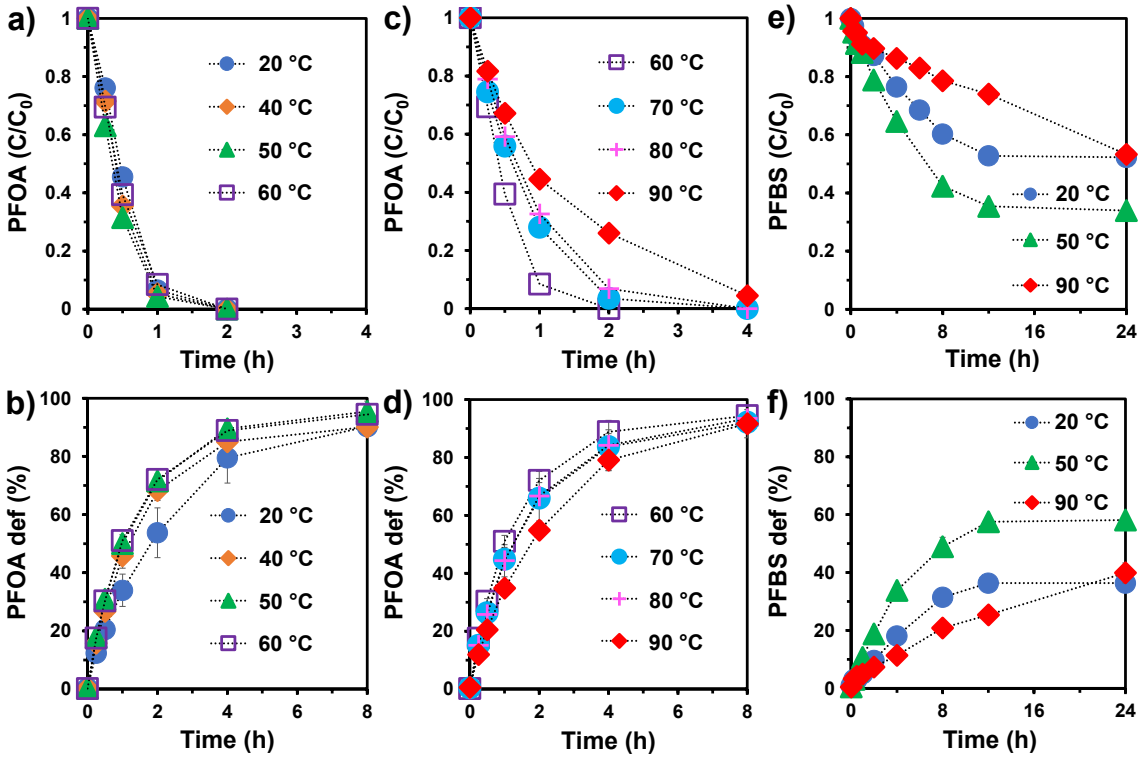

Figure E1. Profiles for (a, c, and e) parent compound decay and (b, d, and f) defluorination of PFOA and PFBS at various temperatures. Reaction conditions: individual PFAS (25 μM), Na_2SO_3 (10 mM), $NaHCO_3$ (5 mM), pH 12.0, and 254 nm irradiation (10 W lamp for 2 L solution).

Table E1. Defluorination Ratio and Rate Constant of PFAS by UV/Sulfite Treatment at 20, 50, and 90°C.[a]

PFCA ($C_nF_{2n+1}COO^-$)	def% after 8 h			decay rate in h^{-1} (decay% after 8 h)		
	20 °C	50 °C	90 °C	20 °C	50 °C	90 °C
n = 1 TFA	99 ± 2.0	99 ± 0.5	96 ± 2.5	2.15 (> 99)	2.60 (> 99)	0.72 (> 99)
n = 2 PFPrA	76 ± 5.7	89 ± 1.5	89 ± 4.2	2.01 (> 99)	2.72 (> 99)	0.81 (> 99)
n = 3 PFBA	92 ± 2.8	95 ± 0.4	94 ± 0.9	1.73 (> 99)	2.92 (> 99)	0.82 (> 99)
n = 4 PFPeA	85 ± 3.0	91 ± 2.5	88 ± 2.5	1.70 (> 99)	2.75 (> 99)	0.83 (> 99)
n = 5 PFHxA	86 ± 0.5	90 ± 0.4	87 ± 4.5	1.50 (> 99)	2.74 (> 99)	0.77 (> 99)
n = 6 PFHpA	83 ± 2.7	86 ± 1.8	85 ± 4.9	1.28 (> 99)	2.19 (> 99)	0.62 (> 99)
n = 7 PFOA	90 ± 0.6	95 ± 3.6	92 ± 4.9	1.58 (> 99)	2.31 (> 99)	0.67 (> 99)
PFSA ($C_nF_{2n+1}SO_3^-$)	**def% after 24 h**			**decay rate in h^{-1} (decay% after 24 h)**		
	20 °C	**50 °C**	**90 °C**	**20 °C**	**50 °C**	**90 °C**
n = 4 PFBS	36 ± 0.5	58 ± 0.2	40 ± 3.5	0.05 (47)	0.09 (66)	0.02 (48)
n = 6 PFHxS	74 ± 2.7	86 ± 2.2	79 ± 0.8	0.27 (> 99)	0.50 (> 99)	0.10 (96)
n = 8 PFOS	88 ± 3.8	89 ± 2.9	87 ± 3.7	0.75 (> 99)	1.22 (> 99)	0.41 (> 99)
FTCA ($C_nF_{2n+1}CH_2CH_2COO^-$)	**def% after 24 h**			**decay rate in h^{-1} (decay% after 24 h)**		
	20 °C	**50 °C**	**90 °C**	**20 °C**	**50 °C**	**90 °C**
n = 4 FTCA	12 ± 0.4	22 ± 1.8	9 ± 0.5	< 0.01 (12)	< 0.01 (21)	< 0.01 (8)
n = 6 FTCA	68 ± 4.1	86 ± 4.5	72 ± 5.7	0.19 (89)	0.35 (> 99)	0.07 (85)
n = 8 FTCA	78 ± 4.4	86 ± 2.6	86 ± 4.0	0.58 (> 99)	0.79 (> 99)	0.34 (99)

[a]Reaction conditions: individual PFAS (25 μM), Na_2SO_3 (10 mM), $NaHCO_3$ (5 mM), pH 12.0, and 254 nm irradiation (10 W low-pressure Hg lamp for 2 L solution).

The addition of iodide for reaction acceleration also benefited from the elevated temperature to 50°C (Figure E2). However, iodide addition did not alter the PFAS degradation mechanism, so the maximum deF% by UV/sulfite+iodide was the same as by UV/sulfite. The positive effects from both iodide addition and heating to 50°C can synergistically achieve significantly enhanced defluorination performance.

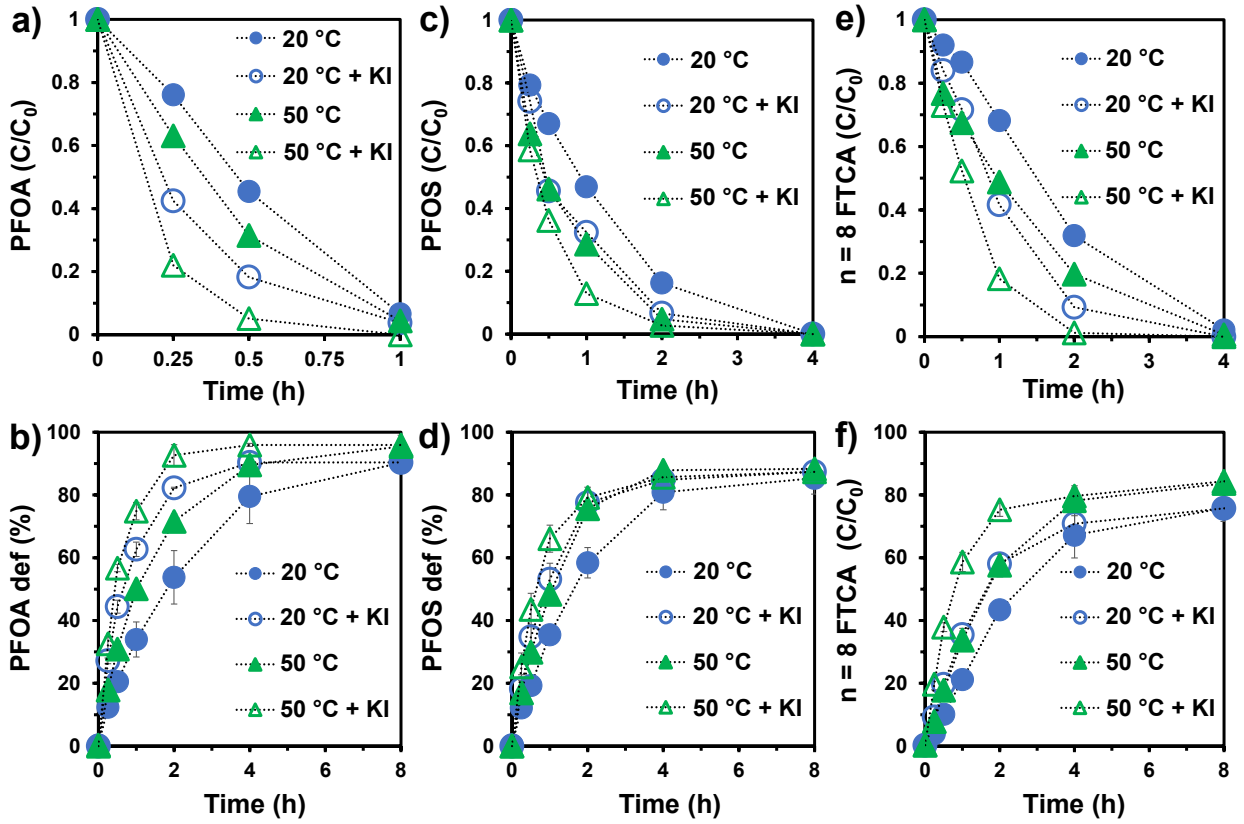

Figure E2. Profiles for (a, c, and e) parent compound decay and (b, d, and f) defluorination of PFOA, PFOS, and n = 8 FTCA with or without KI (2 mM) at 20 °C and 50 °C. Reaction conditions: individual PFAS (25 μM), Na_2SO_3 (10 mM), $NaHCO_3$ (5 mM), pH 12.0, and 254 nm irradiation (10 W low-pressure Hg lamp for 2 L solution).

The **second highlight of this project** is the systematic understanding of the structure-reactivity relationship and mechanisms for non-photochemical, non-redox defluorination of PFAS at elevated temperature and alkaline conditions. We found a series of H-containing PFAS allowed non-redox defluorination under alkaline conditions (pH≥9, Figure E3). The 6:2 FTCA ($C_6F_{13}C\mathbf{H_2}COO^-$) showed limited defluorination at pH 9.0 and 20ºC, primarily via HF elimination (i.e., yielding $C_5F_{11}-CF=C\mathbf{H}-COO^-$). Elevated temperature (up to 90ºC) and pH (up to 14) not only accelerated the reaction rate but also intensified the level of defluorination via additional mechanisms, many of which remain elusive. For example, $C_6F_{13}C\mathbf{H_2}COO^-$ could be further transformed into multiple PFCAs $C_nF_{2n+1}-COOH$ (n=4, 3, 2) as the end products.

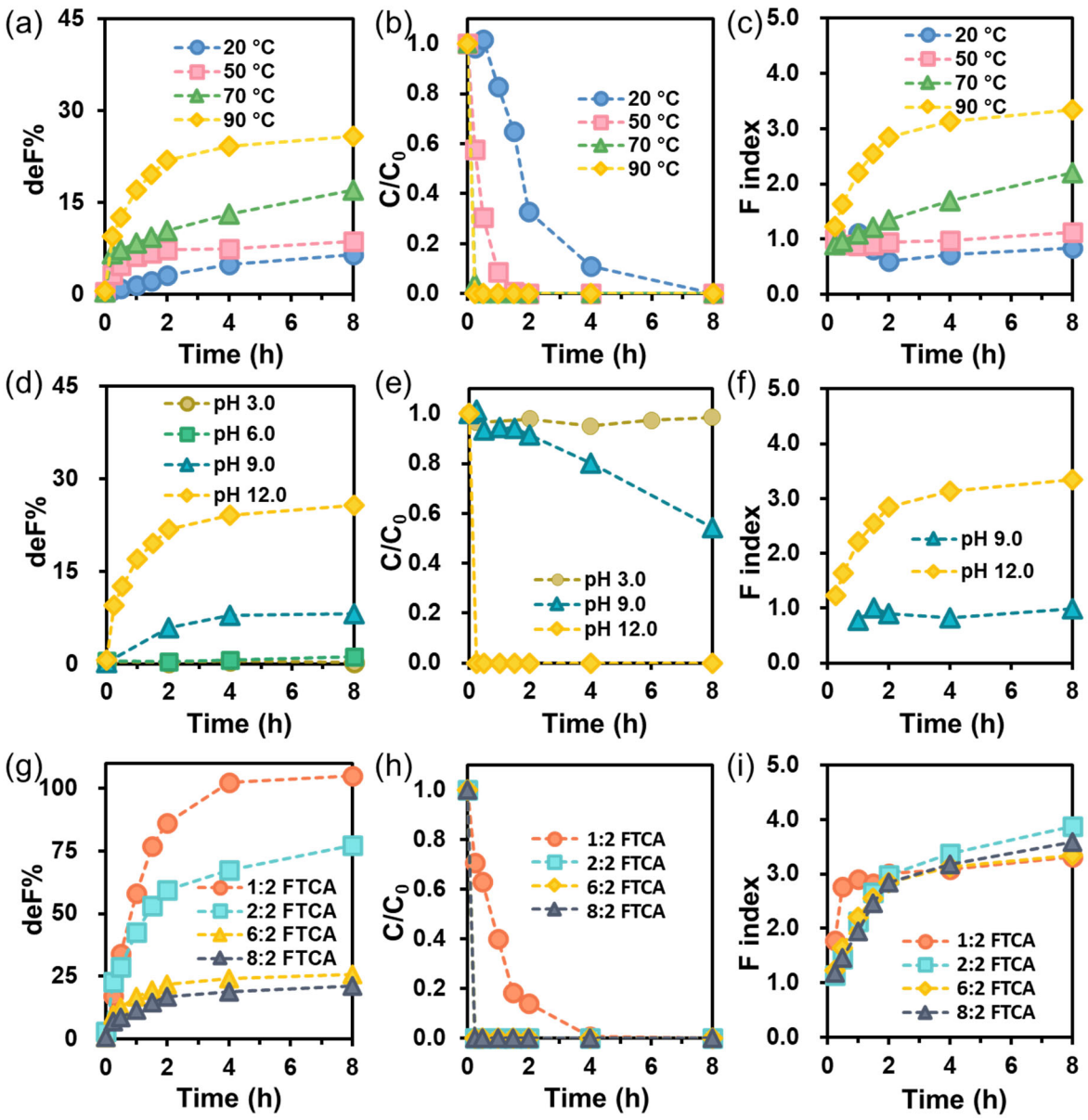

Figure E3. (a-c) Influence of temperature on the defluorination of 6:2 FTCA at pH 12.0; (d-f) Influence of pH on the defluorination of 6:2 FTCA at pH 12.0; (g-i) Defluorination of various n:2 FTCA (n=1, 2, 6, or 8) at pH 12.0 and 90 ºC; [n:2 FTCA] = 25 μM.

We further extended the PFAS collection to 30+ H-containing PFAS structures (Table E2) and confirmed the general trend that C−H bonds with a high acidity are prone to be eliminated alongside neighboring F atoms. The resulting double bonds containing F atoms could be further defluorinated by OH^- attacks. Because of the structure specificity, heating the water at pH 12 after UV/sulfite treatment cannot replace oxidation treatment to achieve 100% defluorination for a majority of PFAS. However, the findings provide important insights into the additional PFAS degradation mechanism under heated alkaline conditions (e.g., UV/sulfite at pH 12 without temperature control) and caution the analytical researchers on sample preservation to avoid gradual defluorination in alkaline solutions.

Table E2. Defluorination Performance of Various Polyfluoroalkyl Substances. [a]

entry	PFAS structure	deF%[a] [# of C-F bonds broken per molecule]	Parent compound decay rate (h^{-1})	deF% (10 M NaOH, 90°C, 2 d)
Influence of chain length of n:2 FTCA				
1	1:2 FTCA	103.5±2.12% [3.19±0.15/3F]	1.21±0.06	-
2	2:2 FTCA	83.1±8.06% (4.13±0.38/5F)	depleted in 15 min (> 11.96 h^{-1})	-
3	6:2 FTCA	25.75% [3.35/13F]	depleted in 15 min (> 11.96 h^{-1})	-
4		17.00% (@ 70 °C) [2.21/13F]	12.61	14.6%
5		8.61% (@ 50 °C) [1.12/13F]	3.18±0.32	-
6		7.67% (@ 20 °C) [0.844/13F]	1.77±0.58	-
7	8:2 FTCA	21.1% [3.59/17F]	depleted in 15 min (> 11.96 h^{-1})	-
Influence of head group of $C_nF_{2n+1}–CH_2–R$				
11	1:1 SO_3H	86.96% (2.67/3F)	1.45 ± 0.48	66.4%
10	1:1 CHO	80.04±0.49% [2.40±0.01/3F]	defluorination finished in 15 min (v > 11.96)	79.7%
8	1:1 OH	0.14±0.07%	n/d	
9	6:1 OH	0.09±0.08%	n/d	1.2%
12	3:1 NH_2	0.06%	n/d	
13	4:1 NH_2	0.06%	n/d	9.8%
14	7:1 NH_2	0.04%	n/d	4.6%
Influence of C-H bond location				
15	$CF_3CFHCOOH$	8 h 16.20% [3.82/4F]	0.04±0.01	50.6%
16	$HOOC–CF_2–CH_2–COOH$	38.91±0.31% [1.92±0.63/2F]	0.07±0.01	84.5%
17	$HC_6F_{12}COOH$	0%	-	12.0%
18	$CF_3CHFCF_2CH_2OH$	22.15±2.8% [1.32±0.17/6F]	n/d	-
19	$(CF_3)_2CHCH_2COOH$	109% [6.54/6F]	0.27±0.04	91.4%
20	$CH_3CH_2CF_2–COOH$	0.42%	-	1.1%
21	CF_3CF_2COOH	0	-	-
22	$CH_3CHFCOOH$	0.21%	-	-
23	HCF_2COOH	0%	-	82.1%
24	6:2 COOH	0%	-	0.1%
25	6:2 SO_3H	0%	-	0.6%

entry	PFAS structure	deF%[a] [# of C-F bonds broken per molecule]	Parent compound decay rate (h^{-1})	deF% (10 M NaOH, 90°C, 2 d)
		Influence double bond		
26	CF_3–CH=CH–CH_2–OH	0.50%	n/d	-
27	CF_3–CH=CH–COOH	12 h 1.57±0.05%	−0.01±0.00	-
28	C_3F_7–CH=CH–COOH	0.07±0.03%	0.01±0.00	20.3%
29	CF_3–CF_2–CF=CF–COOH	35.71% @ 12 h [6.44±2.2/7F]	0.10±0.03	21.6%
30	C_5F_{11}–CF=CH–COOH	19.75% [2.37/12F]	1.75±0.58	-
32	CF_2=CF–CH_2–CH_2–COOH	3.89% @ 12 h [0.58/3F]	0.03±0.051	-

[a]Unless specified otherwise, the reaction conditions are pH 12.0 and 90°C and the deF% were obtained at the end of the reaction.

The **third highlight of this project** is the proof-of-concept that the UV lamp can be used as the main source of heat to achieve enhanced defluorination in both reaction rate and depth of destruction. The results reflected the overall effect of thermal energy generation and UV irradiation by low-pressure UV lamps on PFAS degradation. With the 2 L reactors used in this study, two 10 W UV lamps provided the most cost-effective treatment of both PFOA and PFBS (Figure E4).

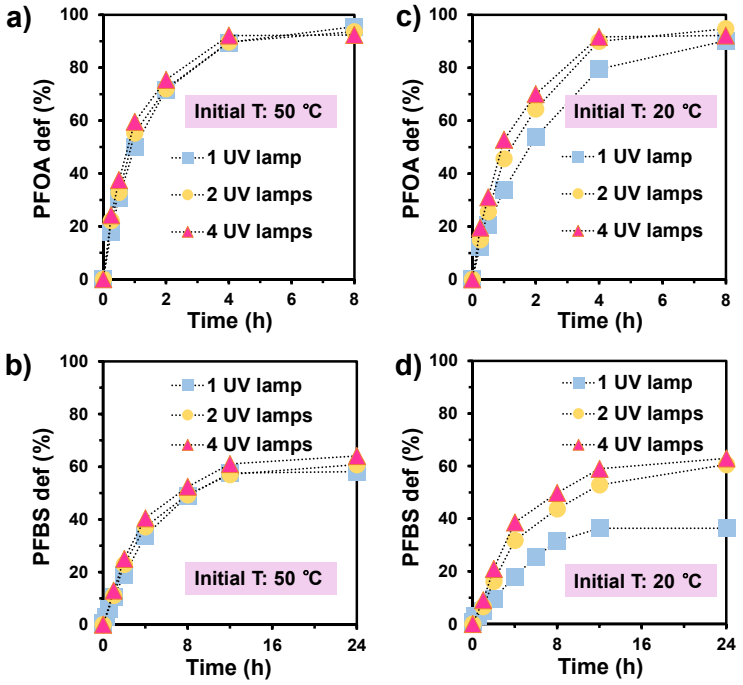

Figure 17. Time profiles for PFOA and PFBS defluorination at the initial temperature of (a and b) 50 °C and (c and d) 20 °C. Reaction conditions: individual PFAS (25 μM), Na_2SO_3 (10 mM), $NaHCO_3$ (5 mM), pH 12.0, and 254 nm irradiation (10 W low-pressure Hg lamps for 2 L solution). No cooling water was used.

The thermal energy from UV lamps is sufficient to bring the water temperature to the optimal 50°C (Table E3), which allows deeper defluorination of the recalcitrant PFBS. Preheating the water to the optimal temperature is not necessary if considering the electrical energy consumption (Table E4). Overall, the heat dissipated from the UV lamps provides significant enhancement in the rate and extent of PFAS defluorination.

Table E3. Water Heating by UV Lamps.[a]

Number of UV lamps	Temperature of water (2 L)			
	Start @ 20 °C		Start @ 50 °C	
	@ 4h	@ 8h	@ 4h	@ 8h
1	36 °C	36 °C	50 °C	50 °C
2	48 °C	53 °C	53 °C	53 °C
4	65 °C	73 °C	73 °C	73 °C

[a]When one 10 W UV lamp was used, a heating plate was needed to achieve the water temperature at 50°C. With two and four UV lamps, a heating plate was not used after the lamps were turned on.

Table E4. Energy Consumption to Achieve Maximum PFAS Defluorination with Varying Numbers of UV Lamps.[a]

Number of UV lamps	Energy consumption to achieve maximum defluorination (kJ for 2 L and kWh/m^3)			
	Start @ 20 °C[b]		Start @ 50 °C[c]	
	PFOA	PFBS	PFOA	PFBS
1	144 (20)	432 (60)	390 (54.2)[d]	678 (94.2)[d]
2	288 (40)	864 (120)	534 (74.2)	1110 (154.2)
4	576 (80)	1728 (240)	822(114.2)	1974 (274.2)

[a]Reaction conditions: PFAS (25 μM), Na_2SO_3 (10 mM), $NaHCO_3$ (5 mM), pH 12.0, and 254 nm irradiation (10 W low-pressure Hg lamp for 2 L solution).
[b]The energy consumption is calculated as n×t×36, where n represents the number of UV lamps, t denotes the time required to reach maximum defluorination (h), and 36 represents the energy consumption per hour by a 10 W UV lamp (kJ).
[c]The energy consumption is calculated as 245.5+n×t×36, where 245.5 represents the energy consumption for heating 2 L of water from 20°C to 50 °C (kJ).
[d]Estimating the energy consumption required to maintain the temperature at 50°C is not straightforward and not included here. This value could greatly vary by thermal insulation settings, which was not studied by this project except for aluminum foil wrapping outside the reactor.

Key Information for Site Managers

1. Elevating the temperature facilitates e_{aq}^- in cleaving the C–F bonds but decreases the quantum yield of e_{aq}^-. Consequently, the overall deF% reached the maximum at 50 °C, where the positive effect outweighed the negative effects to the greatest extent. In practical applications, it is essential to consider the energy consumed in raising the temperature to 50 °C. In our study involving 2 L water and a 10 W light source, the thermal energy needed to heat the water from 20 to 50 °C (without heat dissipation) is comparable to the electrical energy for the UV lamp working over 6.8 h (see main text for details). Hence, it is not advisable to raise the temperature to 50 °C for wastewater mainly containing PFAS structures that are easily degradable, such as PFCAs, PFOS, and n=8 FTCA.
2. The final decay% and deF% enhancement at 50 °C is particularly substantial for short-chain PFSAs and FTCAs, which possess relatively strong C–F bonds. In such scenarios, elevating the temperature could be beneficial for wastewaters primarily containing those types of PFAS. Even without using dedicated equipment to heat the water to 50 °C, PFAS defluorination can be enhanced by the rise in temperature by the UV lamps. For example, our 10 W UV lamp raised the temperature of 2 L water from 20 to 36°C within 4 h (without insulation). The deF% of n=6 FTCA and PFHxS in this study (slowly heated from 20 to 36°C) were 26.7% and 17.9% higher, respectively, compared to the systems where temperature was maintained at 20 °C.
3. In cases where the reaction temperature is elevated excessively (e.g., > 90 °C if a high-power medium/high-pressure Hg lamp is used or multiple low-pressure Hg lamps are used), a cooling operation may be needed to facilitate the optimal PFAS defluorination.
4. The overlooked heat from UV lamps could greatly aid in PFAS defluorination. For the 2 L reactor used in this study, two 10 W UV lamps proved to be the most efficient configuration. For larger reactor designs, temperature control is very important to ensure the water temperature is within the range for optimal defluorination performance. The cooling water setting for academic research (toward a good temperature control at the commonly adopted 20°C across literature) should not be used for practical applications. Instead, thermal insulation should be applied to the reactor parts to preserve the unavoidable heat from UV lamps. In addition, extra heating equipment might be necessary, depending on the number of UV lamps to be used. The detailed parameters need to be determined when pilot- or full-scale reactors are built.
5. The strong electronegativity of the F atom increases the acidity of the H atom in the polyfluoroalkyl structures, making it prone to attack by aqueous OH^-, allowing HF elimination and further transformations. Besides, the F atom on double bonds is also subject to defluorination under alkaline conditions. These findings provide deeper insights into PFAS transformation in both natural and engineering systems. It is important to consider that H-containing PFAS released into the environment or generated from the transformation of other PFAS may undergo spontaneous defluorination.
6. It is highly worth noting that PFAS stock solutions and reaction samples of H-containing PFAS might be unstable under alkaline conditions. For such chemicals (we have provided a large variety of examples in this project), the common practice of using excess NaOH to help dissolve/stabilize acid-type PFAS should be used with caution.

Implications of Future Research and Benefits

The findings have answered most research questions proposed for this limited-scope project. It has confirmed the positive effect of thermal energy, which is the dominant way of electrical energy dissipation from UV lamps (i.e., all energy not utilized for chemical reaction will eventually transform into heat). The findings have been provided to the ESTCP project (ER21-5152) on the treatment of still bottom brines and foam fractionation concentrates and other real PFAS-containing hazardous material treatment cases.

Because of the structure specificity, heating the water at pH 12 after UV/sulfite treatment cannot replace oxidation treatment to achieve 100% defluorination for a majority of PFAS. However, the findings provide important insights into the additional PFAS degradation mechanism under heated alkaline conditions (e.g., UV/sulfite at pH 12 without temperature control) and caution the analytical researchers on sample preservation to avoid gradual defluorination in alkaline solutions. Detailed mechanisms, particularly how the hydroxide attack on the double bond could trigger deeper degradation and eventually form PFCAs in various lengths, remain elusive. Further understanding of such mechanism can be of high value to (1) develop new PFAS degradation technologies using low-cost chemicals and (2) achieve a deeper understanding of PFAS transformation in natural and engineered photochemical systems and microbial systems. Particularly, whether a defluorination step requires the participation of photochemical/biological species (e.g., radicals/enzymes) or simply an alkaline media.

This study did not further test the better-insulated reactors (e.g., using plastic foams or glass wools outside the container rather than aluminum foil) because the pilot- and full-scale systems will have more comprehensive considerations and design guidelines on the heat transfer aspects, such as (1) what part(s) of the system (e.g., reservoir, pipes, and UV module) can be insulated and (2) whether controlled heating and cooling modules are still required from the engineering perspectives. Thus, in this study, we primarily focus on the temperature values and the proof-of-concept rather than developing detailed approaches for heat transfer control.

1. Objective

The overall objectives of this limited-scope project are to obtain a comprehensive understanding and determine key parameters for the thermal-enhanced reductive and alkaline destruction of PFAS. The direct technical goal is to use a limited amount of thermal energy (i.e., heating the water up to 90°C) to enhance the treatment effectiveness and energy efficiency for PFAS degradation. The outcomes validate the "thermal-enhanced" treatment strategy and will benefit the management of PFAS-enriched waste streams in practical demonstration projects.

Three specific objectives were:

(iv) Achieve deep or near-complete defluorination from a majority of PFAS structures by the thermal-enhanced single-step UV/sulfite treatment;
(v) Achieve rapid decay and deep defluorination of recalcitrant PFAS structures such as short-chain sulfonic acids and fluorotelomers by thermal-enhanced photochemical and alkaline treatment;
(vi) Minimize the consumption of both electricity and chemicals through the thermal-enhanced treatment strategy.

Through this project, we collected a comprehensive set of performance data and advanced the engineering aspects of UV/sulfite technology toward field demonstration operations (ESTCP ER21-5152). We elucidated detailed mechanisms for thermal-enhanced PFAS degradation regarding (1) the optimal temperature at 50°C rather than 90°C, (2) the key photochemical parameters that determine the reaction rate, and (3) the role of hydroxide and structure-reactivity relationship in non-photochemical alkaline defluorination. The findings provide novel perceptions of thermal energy effects in a photochemical system.

In early 2020 (when the research proposal was prepared), we proposed a series of technical questions. Most of them have been answered with experimental data and modeling analysis. With new data and mechanistic insights from this and other projects, some early technical questions were answered elsewhere (marked with *, see results in the Final Report of ER18-1289) or became obsolete (marked with #):

- ***Thermal-enhanced UV/sulfite treatment:*** How does the quantitative relationship between the temperature and kinetics look? Do higher temperatures trigger new pathways for PFAS degradation? Does a medium-pressure lamp (wide emission spectrum) trigger new pathways?[#] What is the minimum dose of Na_2SO_3?[*] What is the upper limit of PFAS concentrations for an effective treatment?[*] Can the optimized reaction conditions achieve 100% defluorination of short-chain sulfonic acids and fluorotelomers? If not, what are the structures of the recalcitrant residues?
- ***Thermal-enhanced alkaline defluorination:*** What structural features allow/favor the alkaline defluorination? How does the relationship among temperature, NaOH concentration, and defluorination kinetics look? Can thermal enhancement help reduce the dose of NaOH? What are the transformation products?
- ***Energy and chemical consumption:*** Considering both photochemical and thermal effects, do medium-pressure lamps (high electrical power, wide emission spectrum) have better energy efficiency than low-pressure lamps (low electrical power, 254 nm)?[#] What is the maximum volume of water a single UV lamp can treat without sacrificing performance? How much is the EE/O for the finalized treatment strategy?

2. Background

Thermal-enhanced UV/sulfite defluorination. Among the recently developed PFAS degradation technologies that can work at ambient temperature and pressure, the UV/sulfite system stands out for its excellent performance and low consumption of chemicals and energy.[1, 2, 3, 4-6] UV/sulfite generates hydrated electrons (e_{aq}^-) that can effectively cleave C–F bonds in PFAS (Eqs. 1 and 2).

$$SO_3^{2-} + h\nu \rightarrow SO_3^{\bullet-} + e_{aq}^- \quad (1)$$

$$C\text{–}F + 2e_{aq}^- + H^+ \rightarrow C\text{–}H + F^- \quad (2)$$

Previously, the PI's lab and many other labs maintained the temperature of UV/sulfite treatment at 20°C or lower using a cooling jacket to simulate typical ambient conditions in natural waters.[2, 3, 4-6] In the absence of the cooling jacket; however, the heat generated by the UV lamp could raise the water temperature, potentially expediting the reaction and improving the defluorination percentage. Hydrothermal treatments, conducted at 350 °C and thus higher pressures, have achieved partial or complete PFAS destruction through diverse reaction mechanisms.[7] When this project was proposed in early 2020, the treatment performance and underlying mechanism regarding temperature effects on PFAS degradation under the UV/sulfite treatment were unknown.

Thermal-enhanced alkaline defluorination. As evidenced by bond dissociation energy (BDE) calculations (Figure 1),[2] the hydrogen atoms within polyfluorinated structures strengthen the nearby C−F bonds compared to corresponding fully fluorinated structures. Hence, these H-rich structures exhibit greater resistance to reduction by e_{aq}^- and some could accumulate throughout the reaction.[2] However, the PI's lab observed spontaneous defluorination from specific H-containing polyfluorinated structures in the presence of elevated temperature (below 100 °C) and alkaline conditions (without UV/sulfite treatment). Under the same conditions, the corresponding fully fluorinated structures showed no reactivity. This phenomenon prompted us to consider that H atoms in polyfluorinated structures might initiate new defluorination mechanisms that are less dependent on the redox processes and C−F BDEs.

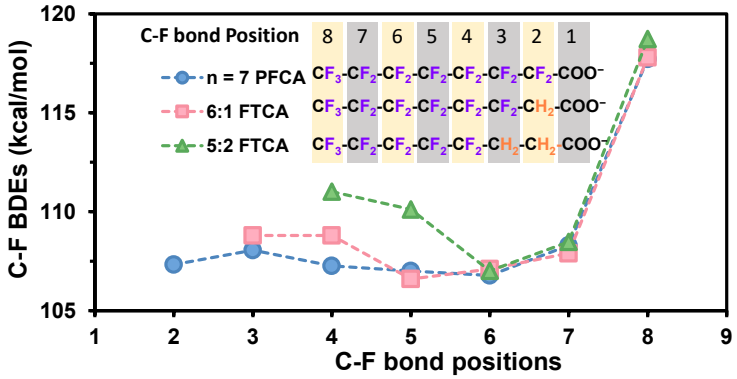

Figure 1. The Influence of C−H bonds on the C−F bond dissociation energies (BDEs, in kcal/mol) in linear PFAS.

Optimize the energy efficiency. It is anticipated that adjusting the number of UV lamps will expedite PFAS defluorination not only because of the irradiation intensity but also due to the temperature change by heat dissipation from UV lamps. When the project was proposed, it was unclear whether adding more UV lamps and removing the cooling system could help cleave additional C–F bonds toward a higher overall defluorination percentage. Adding more UV lamps

entails higher energy consumption, and it was unclear whether this approach could proportionally enhance the rate or extent of PFAS defluorination.

With the knowledge gaps presented above, for this project, we primarily aimed to elucidate the reaction mechanisms underlying the thermal enhancement of PFAS degradation, with (Task 1) or without (Task 2) UV/sulfite treatment, and to further optimize energy efficiency by determining the optimal reaction temperature and the number of UV lamps (Task 3).

3. Materials and Methods

Chemicals and the Preparation of PFAS Stock Solutions. All PFAS chemicals were purchased from Alfa-Aesar, Acros Organics, Oakwood Chemicals, Enamine, Appolo Scientific, and SynQuest Laboratories. Sodium sulfite (Na_2SO_3), potassium iodide (KI), sodium bicarbonate ($NaHCO_3$), sodium hydroxide (NaOH), and sulfuric acid (H_2SO_4) were purchased from Fisher Chemical. Details of chemicals are described in the Appendix. Individual PFASs were dissolved in either deionized (DI, produced by Milli-Q system) water as 10 mM stock solutions. All PFAS stock solutions were stored at 4°C.

Photochemical reactor settings. Low-pressure mercury lamps were placed in a quartz sleeve (Figure 2). Before the reaction, the reactor is loaded with 2000 mL DI water and then placed on a stirring hotplate to heat to the desired temperature. A temperature probe was used to monitor the temperature change. During the reaction, the temperature was maintained at the desired value ± 2 °C. After the desired temperature was reached, 25 μM PFAS, 10 mM Na_2SO_3, 5 mM $NaHCO_3$, and 1.5 mL 10 N NaOH (to adjust the solution pH to 12) were added.[4] Then, the UV lamps were turned on to initiate the reaction. Aliquots of solution (6 mL each) were taken at time intervals.

Figure 2. The photoreactor used for this project.

Experimental settings for thermally enhanced alkaline defluorination. In a 250-mL conical flask, the pH of a 200-mL solution was adjusted to 9.0−12.0 using 10 M NaOH. The solution was heated to 20−90 °C on a stirring hot plate with a temperature probe (Figure 3). PFAS stock solution was added to initiate the reaction. All samples taken at time intervals were quenched by H_2SO_4 (1 M stock solution) to pH 3.0 to avoid further alkaline reactions during storage. Water evaporation had little effect on the concentration of ionizable PFAS structures at neutral or alkaline pH (Figure 4).

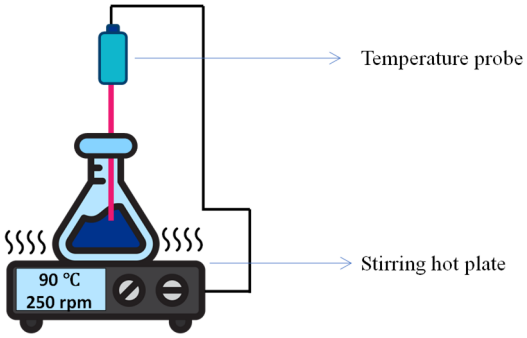

Figure 3. The experimental setup for thermally enhanced alkaline defluorination.

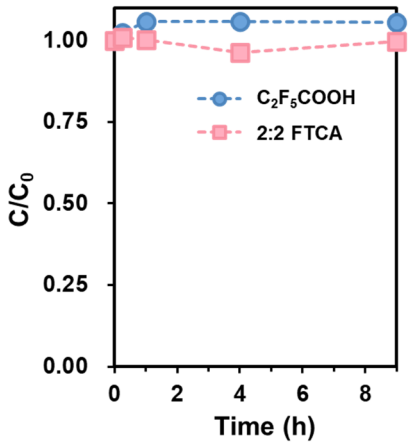

Figure 4. The concentration variation of 25 μM of C_2F_5COOH and 2:2 FTCA ($C_2F_5CH_2COOH$) at 7.0 and 90 ℃.

Fluoride ion (F^-) release during the reaction process was monitored using an ion-selective electrode (ISE, Fisherbrand Accumet) with a Thermo Scientific Orion Versa Star Pro meter. Prior to analysis, each sample (1.5 mL) was mixed with an equal volume of the total ionic strength adjustment buffer (TISAB for fluoride electrode, Thermo Scientific). The accuracy of F^- measurement by ISE was validated by ion chromatography in our previous work.[2] The defluorination percentage (deF%) of PFAS was calculated as the concentration ratio between the released fluoride ion and the total F in the parent PFAS molecule before the reaction, as shown by Eq. 3. The F index value, representing the average number of C−F bonds cleaved per parent compound degraded, was calculated as the concentration ratio between the released F^- and the degraded parent PFAS (Eq. 4).

$$\text{deF\%} = \frac{[F^-]_{release}}{[PFAS]_0 \times N_{C\text{-}F}} \times 100\% \quad (3)$$

$$\text{F index} = \frac{[F^-]_{release}}{[PFAS]_{degraded}} \quad (4)$$

Quantification of parent PFAS. An ultra-high-performance liquid chromatography equipped with a high-resolution quadrupole orbitrap mass spectrometer (UHPLC−HRMS/MS) (Q Exactive, Thermo Fisher Scientific) was used. For UHPLC separation, the mobile phase used (A) 10 mM ammonium acetate in Milli-Q water and (B) 10 mM ammonium acetate in HPLC-grade methanol. A 2-μL sample was loaded onto a Hypersil GOLD column (particle size 1.9 μm, 100×2.1 mm, Thermo Fisher Scientific) and eluted at a flow rate of 300 μL/min. Gradient: 95% A for 0−1 min, 95%−5% A for 1−6 min, 5% A for 6−8 min, and 95% A for 8−10 min. The parent compounds and TPs were detected in full scan negative ionization mode on HRMS at a resolution of 70,000 at m/z 200 and a scan range of m/z 50−750. Data analysis used Freestyle 1.6 and TraceFinder 4.1 EFS (Thermo Fisher Scientific) as described previously.[8, 9]

TP identification. The TPs from each PFAS were identified by suspect screening as described in our previous studies.[8] Briefly, TraceFinder 4.1 EFS (Thermo Fisher Scientific) was used for the product screening. The TP suspect lists were generated by a self-written automatic product mass prediction script. The script was specifically modified to include possible products such as

hydrodefluorination, sulfonation, and decarboxylation products from UV/sulfite treatment. The valid TPs were identified based on the following criteria: (i) mass tolerance < 5 ppm; (ii) isotopic pattern score > 70%; (iii) peak area > 10^5; (iv) peak area showing either an increasing trend or first showing an increasing trend then followed by a decreasing trend over time.

Quality assurance and quality control (QA/QC). The mass detector was calibrated using Pierce ESI Positive/Negative Ion Calibration Solutions (Thermo Scientific) before each analytical run. To take into account the matrix effect on the MS quantitation, we used a PFAS-free solution from the photoreactor (i.e., all inorganic chemicals added and treated under the same UV irradiation) to prepare the calibration standards. The matrix-match standard series comprised eight concentration points ranging from 10 nM to 2.5 μM. No PFASs were detected in the Milli-Q water, pure methanol, and matrix-match blank controls. In order to avoid any PFAS carry over, one Milli-Q water and one methanol blank were also injected between each group of samples and checked for PFAS detection. All samples were stored at 4 °C for less than three weeks before measurement.

Quantification of short-chain organic anions and sulfite. The concentrations of short-chain organic anions and sulfite were analyzed by a Dionex ICS-5000 ion chromatography (IC) system equipped with a conductivity detector and suppressor (AERS 4 mm) and a Dionex ICS-6000 EG eluent generator using an EGC 500 KOH cartridge. The separation of the anions used an IonPac AS11-HC analytical column (4 × 250 mm) in line with an AG11-HC guard column (4 × 50 mm). Specific methods for each analyte are below:

- TFA: Isocratic, 1.0 mL min^{-1}, 10 mM KOH, 30 °C, 30 minutes;
- PFPrA: Isocratic, 1.5 mL min^{-1}, 20 mM KOH, 30 °C, 20 minutes;
- Sulfite: Isocratic, 1.0 mL min^{-1}, 20 mM KOH, 30 °C, 20 minutes.

4. Results and Discussion

4.1 Thermal-enhanced UV/sulfite defluorination

In this section, only one UV lamp was used for all reactions. If the solution temperature began at 20 °C (room temperature), it was gradually heated from 20 to 36 °C within the first 4 h by the UV lamp, then maintained around 36 °C due to heat dissipation balance. We first investigated the effect of temperature on PFAS defluorination below the boiling point of water (20–90 °C). While increased rates and extents of PFAS defluorination were anticipated, when the temperature was elevated over 50 °C, a lowered defluorination performance went beyond our initial expectation. We conducted transformation products (TPs) analysis and calculated the quantum yield of e_{aq}^-, unveiling new mechanistic insights into the temperature effects. The findings contribute not only to the advancement of PFAS remediation technologies but also to filling knowledge gaps in aquatic photochemistry.

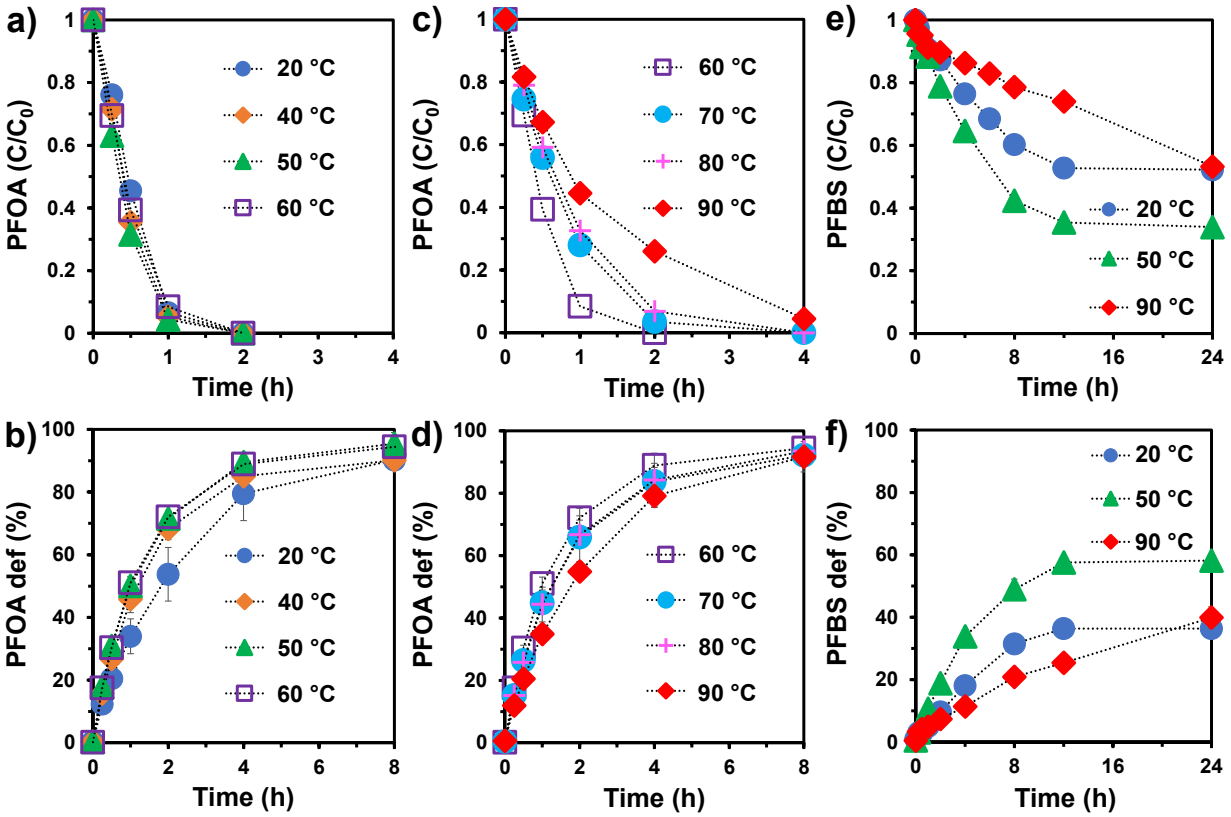

Figure 5. Profiles for (a, c, and e) parent compound decay and (b, d, and f) defluorination of PFOA and PFBS at various temperatures. Reaction conditions: individual PFAS (25 μM), Na_2SO_3 (10 mM), $NaHCO_3$ (5 mM), pH 12.0, and 254 nm irradiation (10 W lamp for 2 L solution).

4.1.1 <u>Temperature effect on PFAS decay and defluorination.</u> We initially selected perfluorooctanoate ($C_7F_{15}COO^-$, PFOA) as the model compound to investigate the temperature effect within the range of 20 to 90 °C. The PFOA decay rate exhibited an increasing trend below 50 °C (Figure 5a), followed by a declined performance as the temperature was elevated further (Figure 5c). The defluorination rate of PFOA followed a similar pattern, reaching its peak at 50 °C and subsequently decreasing with further temperature elevations (Figures 5b and d). We also examined the degradation of other PFAS structures, including n=1–6 perfluorocarboxylates

($C_nF_{2n+1}COO^-$, PFCAs) and n=4, 6, 8 perfluoroalkane sulfonates (PFSAs, $C_nF_{2n+1}SO_3^-$) and fluorotelomer carboxylates (FTCAs, $C_nF_{2n+1}–CH_2CH_2–COO^-$), at temperatures of 20, 50, and 90 °C, respectively (Table 1 and Figures 5e, f and A1–A3). The results confirmed the PFAS decay and defluorination rates exhibit a trend of initially increasing and then decreasing with temperature. Increasing the temperature from 20 to 50 °C improved the PFAS decay rates by 21 to 85% and the final decay percentage (decay%) of n=4 PFSA and n=4 and 6 FTCAs by 9 to 19% (Table 1). However, further elevating the temperature to 90 °C decreased the rates by 41 to 66 % compared to 20 °C, although the final decay% did not change significantly. Compared to 20 °C, PFAS defluorination at 50 °C was both faster and deeper (Table 1). For PFCAs, the most significant difference was observed for n=2 $CF_3CF_2–COO^-$ (PFPrA), with a 13% increase, while n=3–7 PFCAs showed variances ranging from 3 to 7%. The n=1 $CF_3–COO^-$ (TFA) exhibited near-complete defluorination at both temperatures. For PFSAs and FTCAs, the defluorination ratios were substantially enhanced (10–22%) for the short-chain (n=4 and 6) structures, which showed relatively lower degradability.[2] For example, the defluorination ratio of n=4 perfluorobutane sulfonate (PFBS, $C_4F_9SO_3^-$) at 20 °C was 36%, which was enhanced to 58% at 50 °C (Figure 5f). Notably, despite the slower PFAS defluorination rate at 90 °C (Figures 5 and A1–A3), the final defluorination ratio gradually reached a level similar to that at 20 °C (Table 1).

Table 1. Defluorination Ratio and Rate Constant of PFAS by UV/Sulfite Treatment at 20, 50, and 90 °C.[a]

PFCA ($C_nF_{2n+1}COO^-$)	def% after 8 h			decay rate in h^{-1} (decay% after 8 h)		
	20 °C	50 °C	90 °C	20 °C	50 °C	90 °C
n = 1 TFA	99 ± 2.0	99 ± 0.5	96 ± 2.5	2.15 (> 99)	2.60 (> 99)	0.72 (> 99)
n = 2 PFPrA	76 ± 5.7	89 ± 1.5	89 ± 4.2	2.01 (> 99)	2.72 (> 99)	0.81 (> 99)
n = 3 PFBA	92 ± 2.8	95 ± 0.4	94 ± 0.9	1.73 (> 99)	2.92 (> 99)	0.82 (> 99)
n = 4 PFPeA	85 ± 3.0	91 ± 2.5	88 ± 2.5	1.70 (> 99)	2.75 (> 99)	0.83 (> 99)
n = 5 PFHxA	86 ± 0.5	90 ± 0.4	87 ± 4.5	1.50 (> 99)	2.74 (> 99)	0.77 (> 99)
n = 6 PFHpA	83 ± 2.7	86 ± 1.8	85 ± 4.9	1.28 (> 99)	2.19 (> 99)	0.62 (> 99)
n = 7 PFOA	90 ± 0.6	95 ± 3.6	92 ± 4.9	1.58 (> 99)	2.31 (> 99)	0.67 (> 99)
PFSA ($C_nF_{2n+1}SO_3^-$)	**def% after 24 h**			**decay rate in h^{-1} (decay% after 24 h)**		
	20 °C	**50 °C**	**90 °C**	**20 °C**	**50 °C**	**90 °C**
n = 4 PFBS	36 ± 0.5	58 ± 0.2	40 ± 3.5	0.05 (47)	0.09 (66)	0.02 (48)
n = 6 PFHxS	74 ± 2.7	86 ± 2.2	79 ± 0.8	0.27 (> 99)	0.50 (> 99)	0.10 (96)
n = 8 PFOS	88 ± 3.8	89 ± 2.9	87 ± 3.7	0.75 (> 99)	1.22 (> 99)	0.41 (> 99)
FTCA ($C_nF_{2n+1}CH_2CH_2COO^-$)	**def% after 24 h**			**decay rate in h^{-1} (decay% after 24 h)**		
	20 °C	**50 °C**	**90 °C**	**20 °C**	**50 °C**	**90 °C**
n = 4 FTCA	12 ± 0.4	22 ± 1.8	9 ± 0.5	< 0.01 (12)	< 0.01 (21)	< 0.01 (8)
n = 6 FTCA	68 ± 4.1	86 ± 4.5	72 ± 5.7	0.19 (89)	0.35 (> 99)	0.07 (85)
n = 8 FTCA	78 ± 4.4	86 ± 2.6	86 ± 4.0	0.58 (> 99)	0.79 (> 99)	0.34 (99)

[a]Reaction conditions: individual PFAS (25 μM), Na_2SO_3 (10 mM), $NaHCO_3$ (5 mM), pH 12.0, and 254 nm irradiation (10 W low-pressure Hg lamp for 2 L solution).

4.1.2 Insights from molecular transformation. We conducted TP analysis to understand the effect of temperature on PFAS degradation. For n=7 PFOA, the generation and the following degradation of $C_7F_{14}H–COO^-$ (from hydrodefluorination,[2] Figure 6a), $C_7F_{14}(SO_3^-)–COO^-$ (from sulfonation,[6] Figure 6b) and $C_6F_{13}–COO^-$ (from decarboxylation,[2] Figure 6c) were faster at 50 °C compared to 20 °C. The time required for these TPs to reach maximum peak intensities was shortened from 1 to 0.5 h (or 0.25 h). The maximum peak intensities for these TPs were almost the same at 50 °C and 20 °C. However, we note that the detected concentration of a TP reflects the balance between its generation and degradation occurring at the same time. That is, the total generated amounts of these TPs at 50 °C should be more than those at 20 °C. The same trend was observed for the short-chain n = 3 $C_3F_7–COO^-$ (PFBA) (Figure 7).

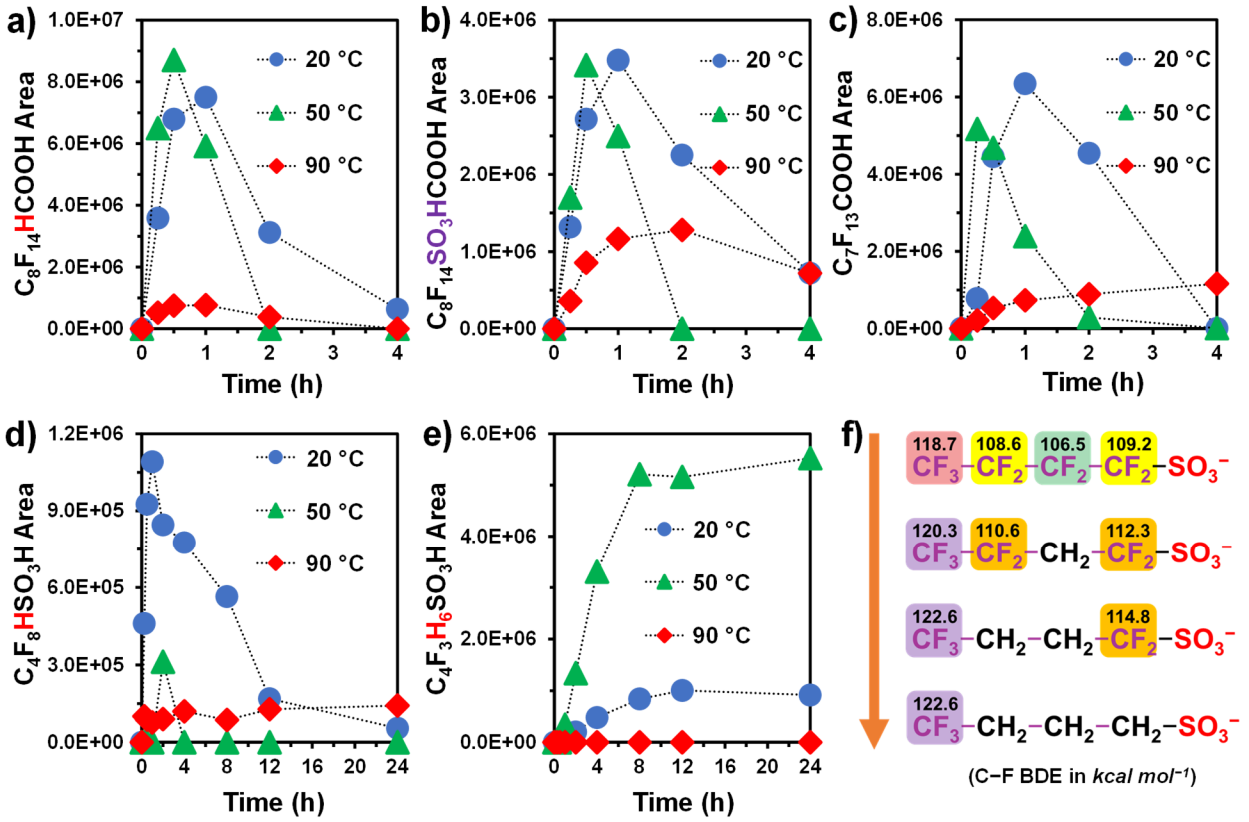

Figure 6. Time profiles for TPs formation from (a, b, and c) PFOA and (d and e) PFBS; (f) the change of calculated C–F BDEs at the B3LYP-D3(BJ)/6-311+G(2d,2p) level of theory for H/F exchange TPs from PFBS. Reaction conditions: individual PFAS (25 μM), Na_2SO_3 (10 mM), $NaHCO_3$ (5 mM), pH 12.0, and 254 nm irradiation (a 10 W low-pressure Hg lamp for 2 L solution).

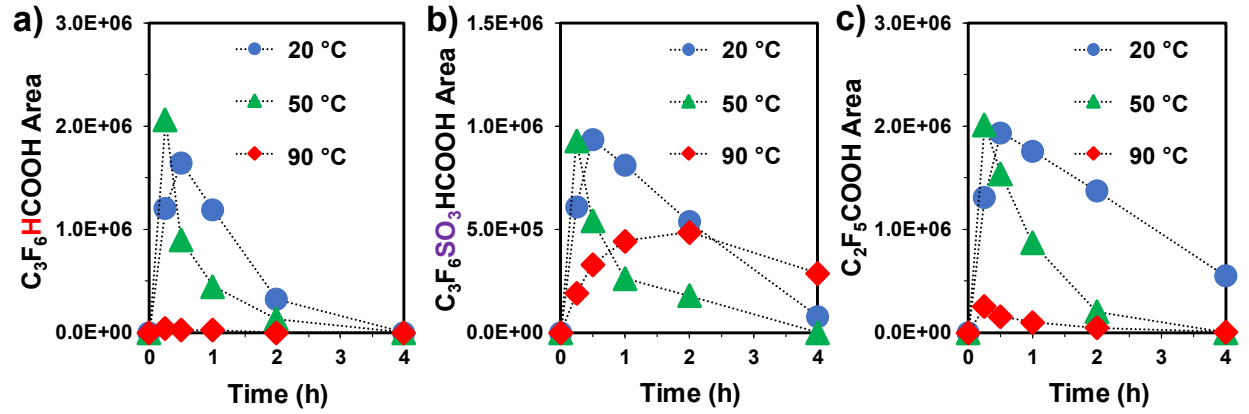

Figure 7. Time profiles for TPs formation from PFBA. Reaction conditions: PFBA (25 μM), Na_2SO_3 (10 mM), $NaHCO_3$ (5 mM), pH 12.0, and 254 nm irradiation (a 10 W low-pressure Hg lamp for 2 L solution).

We further compared the TPs from the degradation of PFBS, which exhibited relatively lower degradability (Table 1).[2] Only hydrodefluorination TPs were observed, likely because of the rapid degradation of other TPs (e.g., PFBA).[2, 10] At 20 °C, a considerably higher amount of C_4F_8H–SO_3^- (single H/F exchange TP, Figure 6d) was observed compared to 50 °C, and $C_4F_7H_2$–SO_3^-

(double H/F exchange TP, Table 2) was exclusively detected at 20 °C. However, the observation of $C_4F_3H_6–SO_3^-$ (sextuple H/F exchange TP, Figure 6e) was one order of magnitude higher at 50 °C. This is probably because the faster reaction at 50 °C is not favorable for the accumulation of $C_4F_8H–SO_3^-$ and $C_4F_7H_2–SO_3^-$, and they quickly converted to $C_4F_3H_6–SO_3^-$ (Figure 6f). According to the calculated C–F BDEs for PFBS (Figure 6f), the most probable location for the initial hydrodefluorination is on the β carbon. Further hydrodefluorination generates $–CH_2–$ moieties in the molecular skeleton, strengthening the remaining C–F bonds. To generate $C_4F_3H_6–SO_3^-$, C–F bonds with BDE>114 kcal mol^{-1} must be cleaved. The fact that we observed much more $C_4F_3H_6–SO_3^-$ generated at 50 °C (Figure 6e) indicates that elevated temperature can facilitate in overcoming the activation energy for cleaving the even stronger C–F bonds. This also accounts for the 22 % difference in PFBS defluorination percentage between 50 °C and 20 °C (Table 1). Even at 50 °C, e_{aq}^- is incapable of directly cleaving the strong C–F bonds (i.e., BDE>120 kcal mol^{-1}) in $C_4F_3H_6–SO_3^-$, leading to the accumulation of this TP during the reaction (Figure 6e). In summary, elevating the temperature from 20 °C to 50 °C not only accelerated the reaction but also facilitated the cleavage of strong C–F bonds, resulting in faster and deeper defluorination. When the temperature was elevated to 90 °C, the TPs observed were substantially less than those at 20 °C and 50 °C (Figures 6a–e). This can be attributed to the slower reaction rate at 90 °C (Table 1). To elucidate this counterintuitive phenomenon, we further calculated the quantum yield of e_{aq}^- at various temperature levels.

Table 2. Quantification or Peak Areas of **$C_4F_7H_2SO_3H$** from PFBS Degradation at 20 °C, 50 °C, and 90 °C[a]

Time (h)	peak area of $C_4F_7H_2SO_3H$		
	20 °C	50 °C	90 °C
0	ND[a]	ND	ND
0.25	ND	ND	ND
0.5	ND	ND	ND
1	ND	ND	ND
2	ND	ND	ND
4	1.25E+05	ND	ND
8	1.46E+05	ND	ND
12	ND	ND	ND
24	ND	ND	ND

[a]Reaction conditions: PFBS (25 μM), Na_2SO_3 (10 mM), $NaHCO_3$ (5 mM), pH 12.0, and 254 nm irradiation (10 W low-pressure Hg lamp for 2 L solution).

4.1.3 Insights from hydrated electron yield. The quantum yield, defined as the ratio of dissociated sulfite molecules to photons absorbed (Eq. 5), measures the efficiency of sulfite in converting into e_{aq}^- upon UV_{254nm} light absorption (Eq. 1). This value is not influenced by instrument settings. The relationship between e_{aq}^- quantum yield and the sulfite decay rate is shown in Eq. 6.[11]

$$\emptyset = \frac{\text{\# Sulfite molecules dissociated}}{\text{\# Photons absorbed by the system}} \qquad (5)$$

$$r_S = -\emptyset_S \frac{I_0}{V}(1 - e^{-2.303LC_S\epsilon_S}) \qquad (6)$$

In Eq. 6, r_S represents the decay rate of sulfite (M s^{-1}), $\emptyset_S$ is the quantum yield of e_{aq}^- (mol/einstein), I_0 is the photon flux entering the reaction solution (einstein $cm^{-2}s^{-1}$), V is the volume of the reaction solution (L), L is the effective path of radiation (cm), C_S is the sulfite concentration (M), and ϵ_S is the extinction coefficient of sulfite (M^{-1} cm^{-1}). I_0 (2.9×10^{-6} einstein

$cm^{-2}s^{-1}$) and L (3.9 cm) were determined using methods described in Text A1. r_S and ϵ_S were measured at 20, 50, and 90 °C. Interestingly, despite the increase in the extinction coefficient of sulfite with temperature (19.3, 34.3, and 63.0 M^{-1} cm^{-1} at 20, 50, and 90 °C, respectively), the decay rate decreased with temperature (0.095, 0.085, and 0.023 M h^{-1} at 20, 50, and 90 °C, respectively; Figure 8).

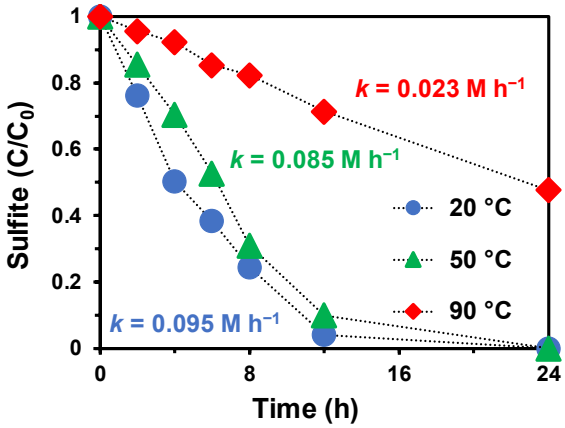

Figure 8. Decay of sulfite at 20 °C, 50 °C, and 90 °C in the absence of PFAS. Reaction conditions: Na_2SO_3 (10 mM), $NaHCO_3$ (5 mM), pH 12.0, and 254 nm irradiation (10 W low-pressure Hg lamp for 2 L solution).

Calculation using Eq. 6 yielded $\emptyset_S$ values of 0.219, 0.171, and 0.044 mol/einstein at 20, 50, and 90 °C, respectively. The significantly reduced $\emptyset_S$ at 90 °C explains the experimentally measured lower PFAS degradation rates. Furthermore, raising the temperature from 20 to 50 °C also decreased $\emptyset_S$. The observed PFAS degradation enhancement at 50 °C indicates that the positive effect of facilitating C–F bond cleavage outweighed the negative effect of generating a smaller amount of e_{aq}^-.

4.1.4 <u>Accelerated defluorination with the addition of iodide.</u> Previously, we observed a substantial enhancement in PFAS degradation by adding iodide into the UV/sulfite system.[10] Elevating the temperature to 50 °C further enhances PFAS decay and defluorination rates within the UV/sulfite + iodide system (Figures 9a–f). Notably, adding iodide and elevating temperature enhanced PFAS defluorination with different mechanisms. Iodide could significantly enhance the availability of e_{aq}^-,[10] while elevating temperature could help overcome the activation energy barrier for C–F bond cleavage. The iodide addition, at either 20 °C or 50 °C, did not increase the maximum deF% (Figures 9b, d, and f), suggesting that UV/sulfite + iodide does not cleave additional C–F bonds that are recalcitrant under UV/sulfite treatment. However, elevating the temperature improved the final deF% by overcoming the reaction barriers (Table 1 and Figures 9b, d, and f). The positive effects of adding iodide and elevating temperature can be synergistically combined (UV/sulfite + iodide at 50 °C) to achieve the highest defluorination efficiency.

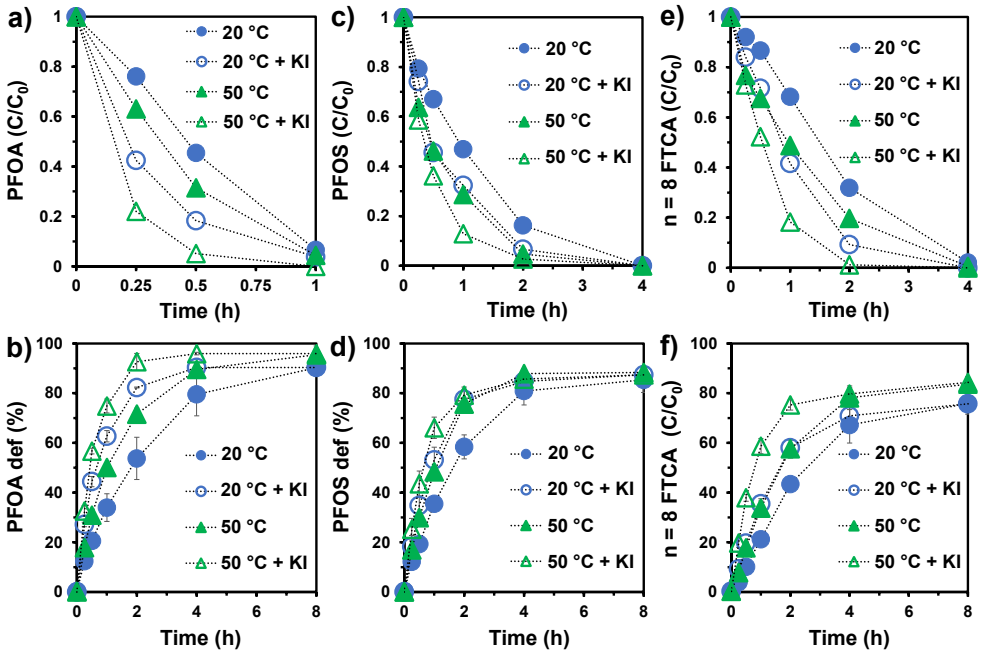

Figure 9. Profiles for (a, c, and e) parent compound decay and (b, d, and f) defluorination of PFOA, PFOS, and n = 8 FTCA with or without KI (2 mM) at 20 °C and 50 °C. Reaction conditions: individual PFAS (25 μM), Na_2SO_3 (10 mM), $NaHCO_3$ (5 mM), pH 12.0, and 254 nm irradiation (10 W low-pressure Hg lamp for 2 L solution).

Table 3. Comparison of deF% in This Study with Those from Our Previous Study.[a]

PFCA ($C_nF_{2n+1}COO^-$)	deF% after 8 h (%)		difference in deF%
	this study (20–36 °C, 10 W, 2L)	previous study (20 °C, 18 W, 0.6 L)	
n = 1 TFA	98.9 ± 2.0	100 ± 2.0	−1.1
n = 2 PFPrA	75.6 ± 5.7	72.9 ± 2.0	2.7
n = 3 PFBA	91.6 ± 2.8	92.2 ± 2.8	−0.6
n = 4 PFPeA	84.7 ± 3.0	78.7 ± 7.7	6.0
n = 5 PFHxA	86.3 ± 0.5	89.3 ± 2.4	−3.0
n = 6 PFHpA	82.9 ± 2.7	83.4 ± 0.8	−0.5
n = 7 PFOA	90.2 ± 0.6	93.0 ± 1.6	−2.8
PFSA ($C_nF_{2n+1}SO_3^-$)	**deF% after 8 h (%)**		**difference in deF%**
	this study (20–36 °C, 10 W, 2L)	**previous study (20 °C, 18 W, 0.6 L)**	
n = 4 PFBS	31.5 ± 0.8	32.4 ± 0.2	−0.9
n = 6 PFHxS	71.3 ± 0.9	53.4 ± 2.3	**17.9**
n = 8 PFOS	85.3 ± 5.1	80.1 ± 1.9	5.2
FTCA ($C_nF_{2n+1}CH_2CH_2COO^-$)	**deF% after 24 h (%)**		**difference in deF%**
	this study (20–36 °C, 10 W, 2L)	**previous study (20 °C, 18 W, 0.6 L)**	
n = 4 FTCA	11.5 ± 0.4	11.3 ± 2.2	0.2
n = 6 FTCA	67.5 ± 4.1	40.8 ± 1.0	**26.7**
n = 8 FTCA	78.3 ± 4.4	76.0 ± 1.0	2.3

[a]Reaction conditions in this study: individual PFAS (25 μM), Na_2SO_3 (10 mM), $NaHCO_3$ (5 mM), pH 12.0, and 254 nm irradiation (10 W for 2 L solution), without cooling water.
Reaction conditions in the previous study[5]: individual PFAS (25 μM), Na_2SO_3 (10 mM), $NaHCO_3$ (5 mM), pH 12.0, and 254 nm irradiation (18 W lamp for 0.6 L solution), with cooling water.

4.1.5 <u>Technical notes for remediation practices.</u> The findings in this section suggest that elevating the temperature facilitates e_{aq}^- in cleaving the C–F bonds but decreases the quantum yield of e_{aq}^-. Consequently, the overall deF% reached the maximum at 50 °C, where the positive effect outweighed the negative effects to the greatest extent. In practical applications, it is essential to consider the energy consumed in raising the temperature to 50 °C. In our study involving 2 L water and a 10 W light source, the thermal energy needed to heat the water from 20 to 50 °C (without heat dissipation) is comparable to the electrical energy for the UV lamp working over 6.8 h (Text A2). Hence, it is not advisable to raise the temperature to 50 °C for wastewater mainly containing PFAS structures that are easily degradable, such as PFCAs, PFOS, and n=8 FTCA. The complete decay and maximum defluorination for these structures were achieved within 8 h at 20°C (Figures 5b, d and A1– A3), with no additional C–F bonds cleaved at 50 °C (Table 1).

However, the final decay% and deF% enhancement at 50 °C is particularly substantial for short-chain PFSAs and FTCAs (Table 1), which possess relatively strong C–F bonds. In such scenarios, elevating the temperature could be beneficial for wastewaters primarily containing those types of PFAS. Even without using dedicated equipment to heat the water to 50 °C, PFAS defluorination can be enhanced by the rise in temperature by the UV lamps. For example, our 10 W UV lamp raised the temperature of 2 L water from 20 to 36°C within 4 h (without insulation). The deF% of n=6 FTCA and PFHxS in this study (slowly heated from 20 to 36°C) were 26.7% and 17.9% higher, respectively, compared to our previous study[5] where the temperature was maintained at 20 °C (Table 3). Notably, the earlier study used a higher UV light power (18 W) and a smaller volume of the reaction solution (600 mL). We also compared the defluorination of other PFAS structures with our previous study[5] but found no significant difference in their deF% (Table 3). Some PFAS structures already exhibited high deF% at 20 °C (PFCAs, PFOS, and n=8 FTCA), while others have a high recalcitrance (PFBS and n=4 FTCA) that require higher temperatures (e.g., 50 °C) for noticeable enhancement of deF% (Table 1).

Lastly, in cases where the reaction temperature is elevated excessively (e.g., > 90 °C if a high-power medium/high-pressure mercury lamp is used or multiple low-pressure mercury lamps are used), a cooling operation may be needed to facilitate the optimal PFAS defluorination.

4.2 Thermal-enhanced alkaline defluorination

To investigate the mechanism of thermal-enhanced alkaline defluorination, we first used n:2 fluorotelomer carboxylic acid (C_nF_{2n+1}−CH_2−COOH, n:2 FTCA) with varying chain lengths (n=1, 2, 6, and 8) as model compounds. We further examined the relationship between defluorination reactivity and the specific chemical structures across 30 types of H-containing PFAS. Our approach included kinetic measurements, model compound experiments, and analysis of TPs. **Note: the experiments in this section did not use UV or sulfite**.

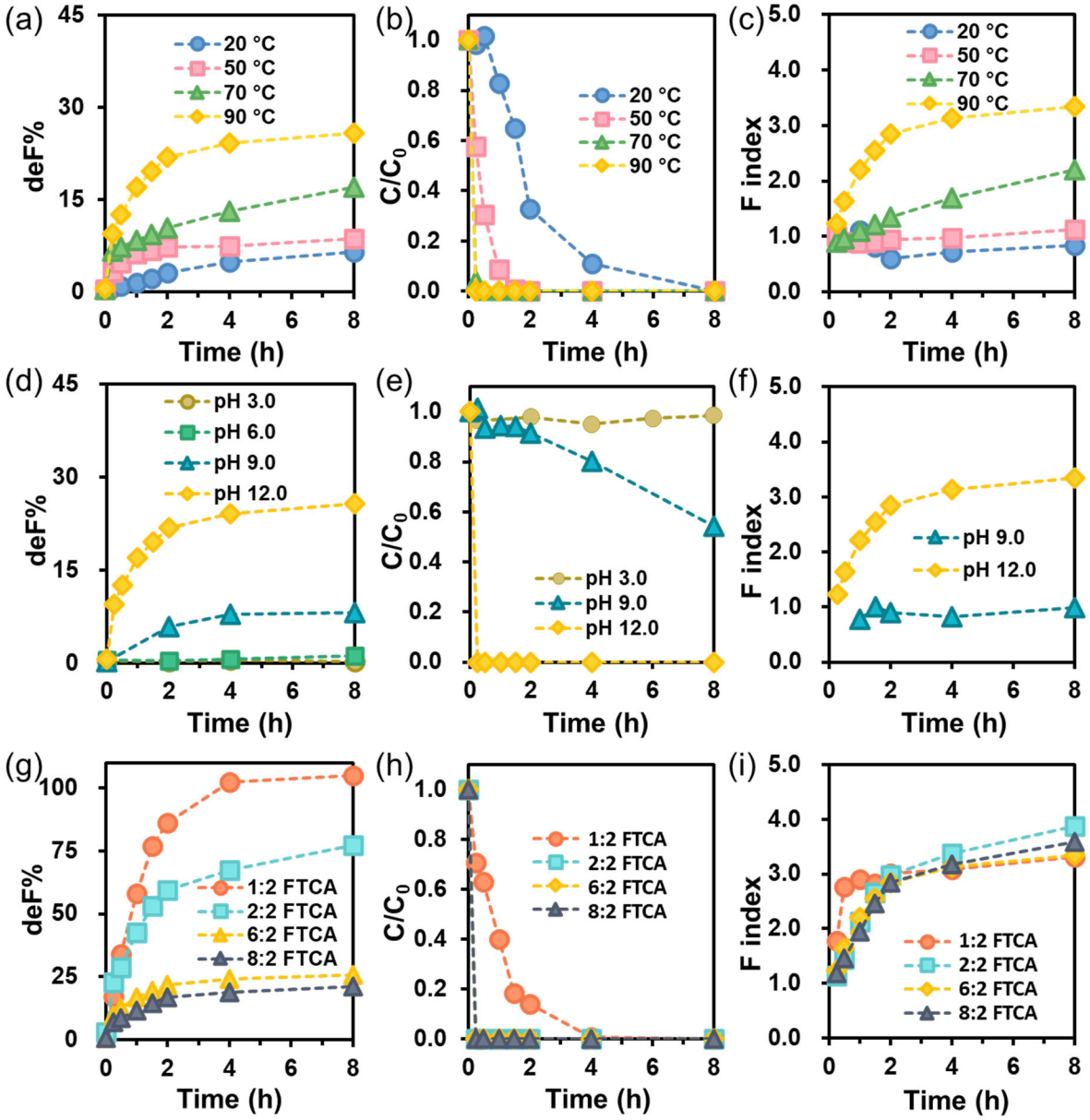

Figure 10. (a-c) Influence of temperature on the defluorination of 6:2 FTCA at pH 12.0; (d-f) Influence of pH on the defluorination of 6:2 FTCA at pH 12.0; (g-i) Defluorination of various n:2 FTCA (n=1, 2, 6, or 8) at pH 12.0 and 90 °C; [n:2 FTCA] = 25 μM.

4.2.1 <u>Alkaline defluorination of n:2 FTCA.</u> We first investigated the Influence of temperature and pH on the alkaline defluorination by using 6:2 FTCA as the model structure. At pH 12.0, defluorination of 6:2 FTCA was observed across all tested temperatures ranging from 20 to 90°C (Figures 10a–c). At room temperature (20°C), complete decay of 6:2 FTCA parent structures was achieved within 8 hours. Increasing the temperature accelerated the defluorination and increased the maximum deF% of 6:2 FTCA. We then maintained the solution temperature at 90°C and examined the Influence of solution pH. The lower pH decreased the defluorination efficacy for 6:2 FTCA, and no defluorination was observed at pH ≤ 6.0 (Figures 10d–f).

By comparing the MS^2 fragments of TPs with corresponding standard chemicals, we identified the first TP from 6:2 FTCA as C_5F_{11}–CF=CH–COOH (*E* configuration) (6:2 FTUCA, Figure A4). This transformation appears to be an HF elimination reaction (–CF_2–CH_2– transformed to –CF=CH–). The HF elimination reaction was the only step that proceeded at relatively low pH (pH 9.0 and 90°C) or low temperature (pH 12.0 and 20°C). This is evidenced by the average C–F bonds broken per degraded parent compound (F index value) being around 1, and 6:2 FTUCA was the only product detected by LC-HRMS/MS. However, deeper defluorination of 6:2 FTCA beyond HF elimination was observed at higher temperatures or higher pH. On average, around three C–F bonds of 6:2 FTCA were cleaved at 90°C and pH 12.0 (F index = 3.3).

We further investigated the alkaline defluorination of n:2 FTCA of other chain lengths (n=1, 2, 8) at pH 12.0 and 90°C (Figure 10g). The degradation of 1:2 FTCA was the slowest, taking 4 hours for complete parent structure decay, but it achieved 100% defluorination. Similar to 6:2 FTCA, both 2:2 FTCA and 8:2 FTCA were completely degraded within 15 min. On average, one C–F bond was cleaved (F index ≈ 1), yielding a great amount of C_nF_{2n+1}–CF=CH–COOH (Figures 11–13). Therefore, the rapid degradation of n>1 n:2 FTCA within the first 15 min was attributed to HF elimination. The final deF% of n>1 n:2 FTCA decreased as the chain length increased, from 83.1±8.1% for 2:2 FTCA to <25% for 6:2 and 8:2 FTCA (Figure 10g).

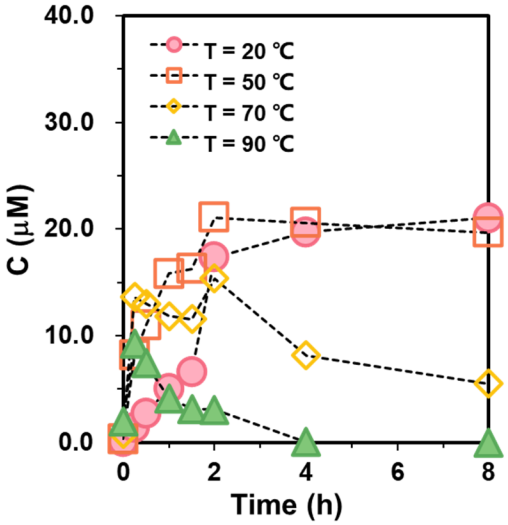

Figure 11. The formation and following degradation of C_5F_{11}–CF=CH–COO^- from 6:2 FTCA at different temperatures.

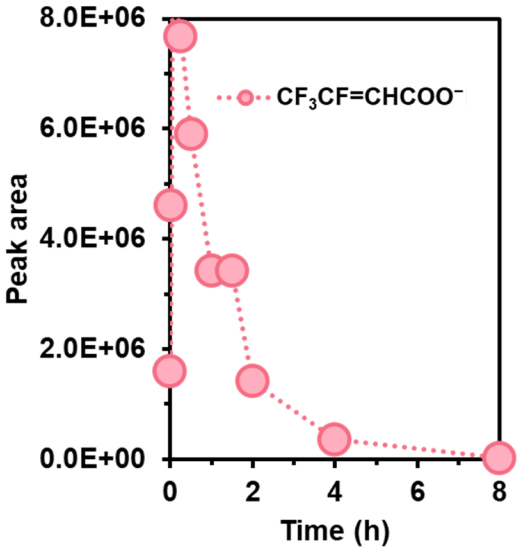

Figure 12. The formation and following degradation of $CF_3{-}CF{=}CH{-}COO^-$ from 2:2 FTCA (pH 12.0 and 90 ºC).

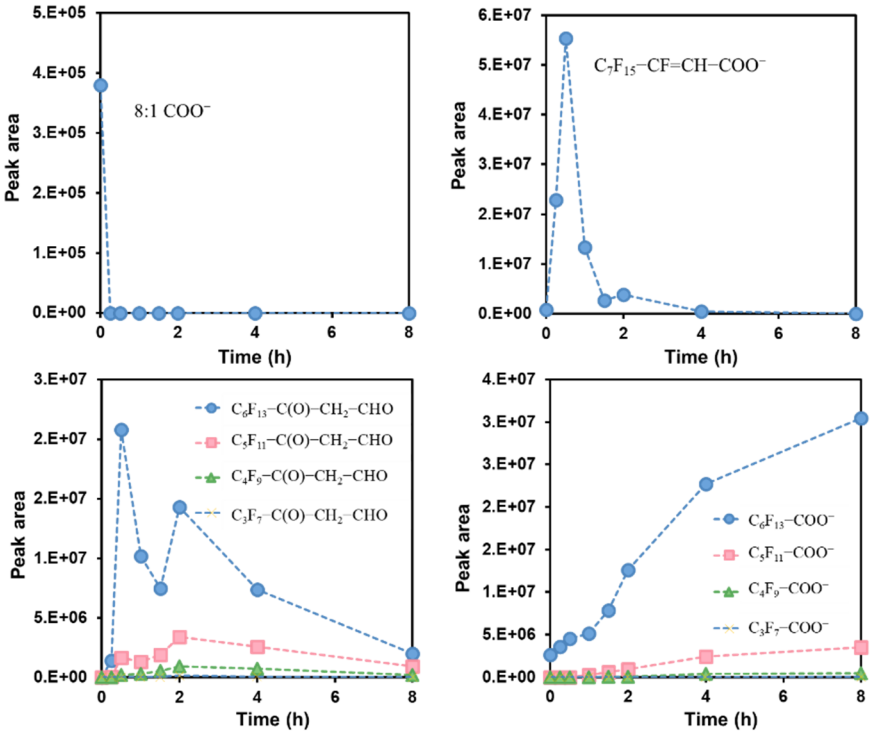

Figure 13. Concentration-time profiles of 8:2 FTCA and its TPs at pH 12.0 and 90ºC.

4.2.2 ***Transformation pathway of 6:2 FTCA.*** The TPs from 6:2 FTCA under 90ºC and pH 12 were investigated with LC−HRMS/MS (Figure 14a). 6:2 FTUCA was the first product, with its concentration reaching a peak at 15 min and then slowly decreasing over the next 4 h. After the complete degradation of 6:2 FTCA at 15 min, we detected a new series of TPs with the chemical formula of $C_nF_{2n+1}{-}C_3H_2O_2H$ (n=4, 3, or 2). The concentrations of all three TPs increased in the beginning and then decreased, with the maximum abundance observed at 2 h. Accompanying the degradation of $C_nF_{2n+1}{-}C_3H_2O_2H$ structures, PFCA ($C_nF_{2n+1}{-}COOH$, n = 4, 3, or 2) were also

generated as the final stable products (Figure 14a). The molecular structures of C_5F_{11}−CF=CH−COOH and PFCAs were confirmed by comparing their MS^2 fragments and retention times in the LC column with corresponding chemical standards (Figure A4).[12] Extra work was performed below to identify the structure of C_nF_{2n+1}−$C_3H_2O_2H$ (n=4, 3, 2).

The TPs of $C_nF_{2n+1}C_3H_2O_2H$ (n = 4, 3, 2) should all have a fully fluorinated skeleton and share the same functional group. This is evidenced by the $C_nF_{2n+1}^-$ and $C_3HO_2^-$ fragments detected in their MS^2 spectra (Figure A5). We initially thought the $C_nF_{2n+1}C_3H_2O_2H$ molecule could be an unsaturated carboxylic acid, i.e., C_nF_{2n+1}−CH=CH−COOH. This structure was also the proposed biological transformation product from C_5F_{11}−CF=CH−COOH in bacterial culture[13] and in animals.[14] However, the commercially available n=1 and n=3 C_nF_{2n+1}−CH=CH−COOH cannot be degraded under our experimental conditions (Figure 14d). Moreover, the retention time and MS^2 fragments of C_3F_7−CH=CH−COOH are different from the $C_3F_7C_3H_2O_2H$ TP detected in our reaction system (Figures A5 and A6).

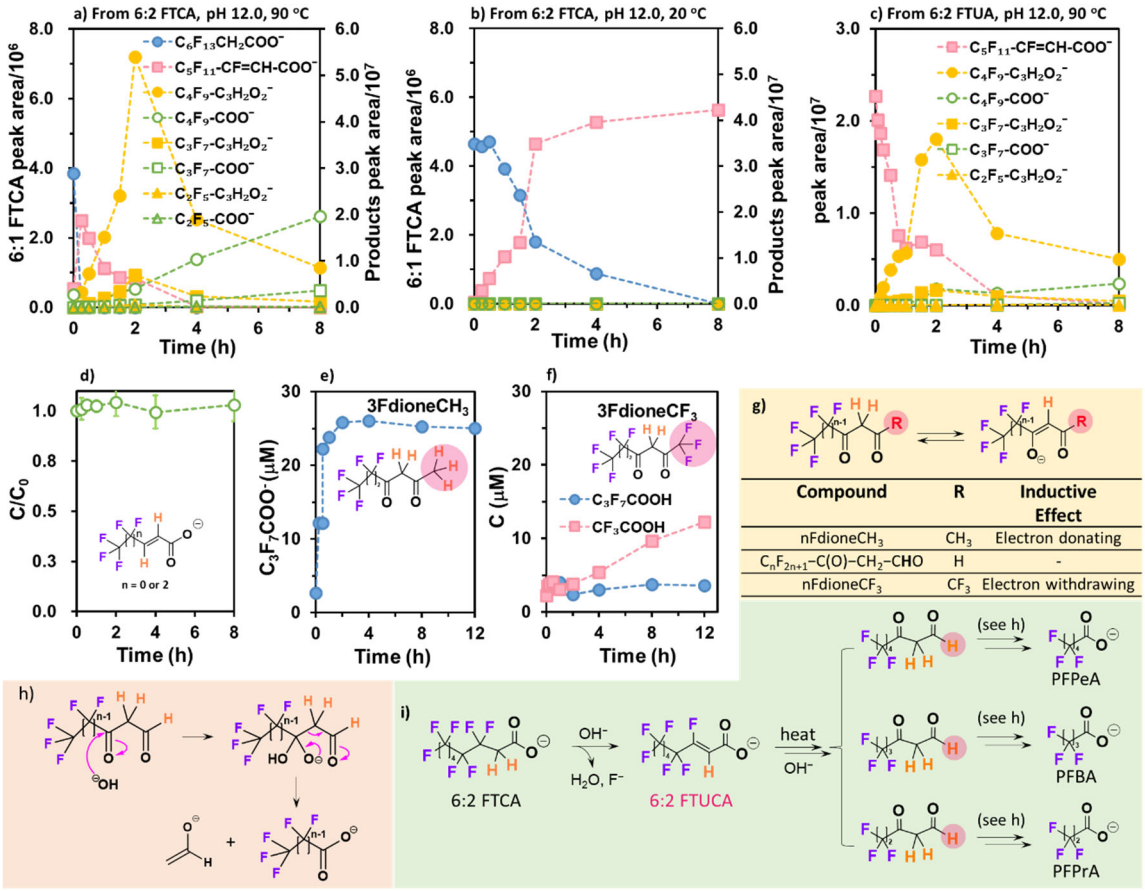

Figure 14. Concentration-time profiles of parent compounds and TPs. Parent compounds: a, b) 6:2 FTCA, c) 6:3 FTUA (C_5F_{11}−CF=CH−COOH), d) C_nF_{2n+1}−CH=CH−COOH, e) $3FdioneCH_3$, and f) $3FdioneCF_3$; g) illustration of the acidic dissociation of C_nF_{2n+1}−C(O)−CH_2−C**H**O, $nFdioneCH_3$, and $nFdioneCF_3$ structures; h) proposed degradation mechanisms for C_nF_{2n+1}−C(O)−CH_2−C**H**O; i) verified transformation pathway of 6:2 FTCA. Reaction conditions: individual PFAS (25 μM), pH 12.0, 90 °C except for panel b (20 °C).

Further investigation revealed the TPs of $C_nF_{2n+1}C_3H_2O_2H$ (n=4, 3, 2) could have the structure C_nF_{2n+1}−C(O)−CH_2−C**H**O. As such structures were not commercially available, we tested two relevant structures, C_nF_{2n+1}−C(O)−CH_2−CO(**CH_3**) (nFdione**CH_3**) and C_nF_{2n+1}−C(O)−CH_2−CO(**CF_3**) (nFdione**CF_3**). The only difference between these three structures is the group/atom connected to the end −C(O)− group (−H in C_nF_{2n+1}−C(O)−CH_2−C**H**O vs −CH_3 in nFdione**CH_3** vs −CF_3 in nFdione**CF_3**, Figure 2g). As compared to −H, the −CF_3 is a strong electron-withdrawing group due to the strong electronegativity of the F atom, while the −CH_3 group is a weak electron-donating group. It is reasonable to assume that the properties of nFdione**CH_3** could be closer to that of C_nF_{2n+1}−C(O)−CH_2−C**H**O. It turns out that all tested nFdione**CH_3** (n=1, 2, 3, and 4) were completely converted to C_nF_{2n+1}COOH at 90 ºC and pH 12 (Figure 15, data of 3Fdione**CH_3** is shown in Figure 14e as an example). This result is the same as the transformation of $C_nF_{2n+1}C_3H_2O_2H$ (n=4, 3, 2) observed in our system. In comparison, nFdione**CF_3** (n = 1, 2, 3, and 4) decayed slowly in 12 h, generating a small amount of C_nF_{2n+1}COOH as well as a considerable amount of CF_3COOH (Figure 15, data of 3FdioneCF_3 are shown in Figure 14f as an example). This conversion was not unexpected, as the highly electronegative −CF_3 group decreases the electron density of the neighboring carbonyl group in nFdione**CF_3**, facilitating the nucleophilic attack of OH^- at this point, thus resulting in the major production of CF_3COOH. All the above results support our hypothesis that the molecular structure of the TPs $C_nF_{2n+1}C_3H_2O_2H$ could be C_nF_{2n+1}−C(O)−CH_2−C**H**O. It has to be noted that although nFdioneCH_3 and nFdioneCF_3 structures do not contain carboxylic groups, they were detected as negative ions by losing an H atom in mass spectrometry (Text A3). This phenomenon also explains why C_nF_{2n+1}−C(O)−CH_2−C**H**O can be detected by the LC-HRMS/MS (the acid dissociation equilibrium was illustrated in Figure 14g).

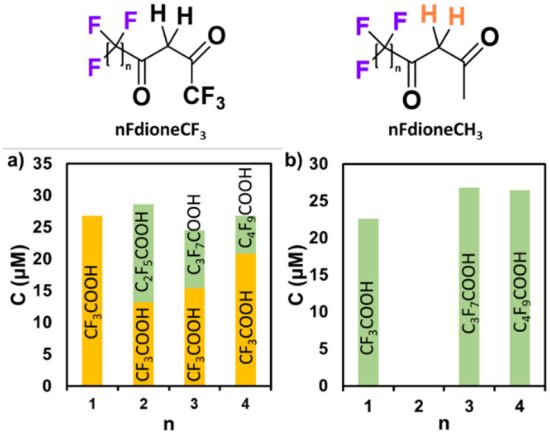

Figure 15. TPs generated from a) nFdioneCF3 and b) nFdioneCH_3 at 90ºC and pH 12.0. $[PFAS]_{ini}$ = 25.0 μM.

The transformation pathways of 6:2 FTCA are summarized in Figure 14i. Briefly, OH^- attacks 6:2 FTCA and yields the HF elimination product, C_5F_{11}−CF=CH−COOH, which then transforms to C_nF_{2n+1}−C(O)−CH_2−C**H**O (detailed steps remain unknown for now). For C_nF_{2n+1}−C(O)−CH_2−C**H**O, OH^- attacks the ketone carbonyl (i.e., next to the C_nF_{2n+1} chain). The −CH_2−CHO group is a better leaving group than −OH,[15] yielding the PFCA as the end product (Figure 14h).

Notably, the transformation pathway scheme shown in Figure 14i is not exclusive, as the fluorine balance at the end of the reaction only reaches ~50% from counting F^- ion and all PFCA

products. We speculate that partial 6:3 FTUA would transform into some stable but non-ionizable TPs and escape the mass spectrometry detection.[13, 14, 16]

4.2.3 <u>Alkaline defluorination of other polyfluorinated structures.</u> The $-CH_2-$ group in n:2 FTCA is a weak point where OH^- can abstract the relatively acidic proton. This reaction further eliminates the neighboring F atom. However, no reaction was observed for $C_nF_{2n+1}-C_2H_4-COOH$ (n:3 FTCA) and $C_nF_{2n+1}-C_2H_4-SO_3H$ (n:2 FTSA) structures under the same condition (90 °C and pH 12.0) or increasing NaOH to 10 M (Table 4, entry 24 and 25). To unravel the structure-reactivity relationship, we tested the defluorination of various polyfluorinated structures under alkaline conditions, with results summarized in Table 4.

<u>a). Influence of head groups</u>. The rate of decay for PFAS bearing CF_3-CH_2- with various head groups (CF_3-CH_2-**R**, entries 11−14 in Table 4) follow the trend **$-CHO > -SO_3H > -COOH$**, with negligible defluorination observed for $C_nF_{2n+1}-CH_2-$**OH** (n=1 or 6, entries 8 and 9) and $C_nF_{2n+1}-CH_2-$**NH_2** (n = 3, 4, or 7, entries 12−14). This trend is roughly correlated with the negative induction effect of the head group, which follows the order $-SO_3^- > -CHO > -COO^- > -OH > -NH_2$.[17] A strong negative induction effect of the head group **R** would lead to higher acidity of the $-CH_2-$ group in the $C_nF_{2n+1}-CH_2-$**R** structure. The low induction effect of −OH and $-NH_2$ results in the low acidity of the $-CH_2-$ group in $C_nF_{2n+1}-CH_2-$**OH** and $C_nF_{2n+1}-CH_2-$**NH_2**, making the protons less likely to be abstracted by OH^- and thus inhibit the HF elimination. The unexpected fast defluorination of CF_3-CH_2-**CHO** might be due to its hydration in water, which will change the acidity of the $-CH_2-$ group.[18]

<u>b). Influence of C-H bond position.</u> Experimental results also demonstrated that the H of high acidity in polyfluorinated structures could be deprotonated for HF elimination. For example, in contrast to the negligible defluorination of $C_nF_{2n+1}-CH_2-OH$ (entry 18 vs entries 8 and 9), around 22.1% defluorination (F index = 1.3 ± 0.2) was observed for CF_3CF**H**CF_2CH_2OH. Moreover, we detected the production of CF_3COOH (Figure 16), which indicates the H on the $-CFH-$ group was eliminated with the F in the middle $-CF_2-$group. This result is consistent with our established knowledge that C−F bonds on the end CF_3 group are much more stable than the C−F bonds within the fluoroalkyl chain.[2] In another example, the omega H on the end group of linear PFAS exhibits low acidity and cannot be eliminated alongside neighboring C−F (entry 17) until the NaOH concentration was elevated to 10 M. This resulted in ~12% defluorination of $HC_6F_{12}COOH$.

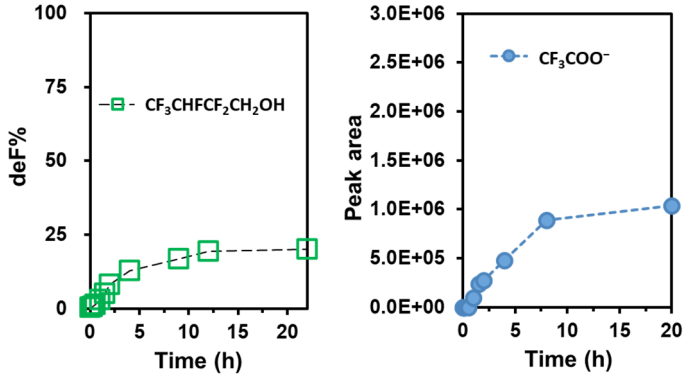

Figure 16. Decay of $CF_3CHFCF_2CH_2OH$ (initial concentration was 25 μM) at pH 12 and 90°C and the production of CF_3COO^-.

The defluorination rate of both **HOOC**−CF_2−CH_2−COOH (entry 16) and CF_3−C**FH**−COOH (entry 15) are slower than CF_3−CH_2−COOH. The F index for HOOC−CF_2−CH_2−COOH is 2 (complete deF), suggesting that the HF elimination TP, HOOC−CF=CH−COOH, is subject to further decomposition. We did not detect any transformation products from CF_3−CFH−COOH, possibly due to their low m/z values falling outside the detection range of our mass spectrometry instrument. Despite the low deF% of CF_3−CFH−COOH (16.2%), a high F index value (3.82) was obtained after 8 h, suggesting the first defluorination as the rate-determining step.

c). Influence of the double bond. According to our previous results, the unsaturated fluorinated structure (C_nF_{2n+1}−CF=CH−COOH) upon HF elimination of n:2 FTCA (n>1) was unstable at pH 12 and T≥50°C, while C_nF_{2n+1}−CH=CH−COOH structure was very stable under at pH 12 and 90 °C (Figure 14d). The atoms on the double bond would substantially influence the structure reactivity. We tested a variety of unsaturated PFAS structures with different combinations of F and/or H on the double bond. The −CF=CF− structure showed the highest defluorination reactivity under alkaline conditions (entry 29 and entry 32), followed by −CF=CH− (entry 26), and −CH=CH− is the least reactive (entry 30).

Table 4. Defluorination Performance of Various Polyfluoroalkyl Substances. [a]

entry	PFAS structure	deF%[a] [# of C-F bonds broken per molecule]	Parent compound decay rate (h^{-1})	deF% (10 M NaOH, 90°C, 2 d)
Influence of chain length of n:2 FTCA				
1	1:2 FTCA	103.5±2.12% [3.19±0.15/3F]	1.21±0.06	-
2	2:2 FTCA	83.1±8.06% (4.13±0.38/5F)	depleted in 15 min (> 11.96 h^{-1})	-
3	6:2 FTCA	25.75% [3.35/13F]	depleted in 15 min (> 11.96 h^{-1})	-
4		17.00% (@ 70 °C) [2.21/13F]	12.61	14.6%
5		8.61% (@ 50 °C) [1.12/13F]	3.18±0.32	-
6		7.67% (@ 20 °C) [0.844/13F]	1.77±0.58	-
7	8:2 FTCA	21.1% [3.59/17F]	depleted in 15 min (> 11.96 h^{-1})	-
Influence of head group of C_nF_{2n+1}−CH_2−R				
11	1:1 SO_3H	86.96% (2.67/3F)	1.45 ± 0.48	66.4%
10	1:1 CHO	80.04±0.49% [2.40±0.01/3F]	defluorination finished in 15 min (v > 11.96)	79.7%
8	1:1 OH	0.14±0.07%	n/d	
9	6:1 OH	0.09±0.08%	n/d	1.2%
12	3:1 NH_2	0.06%	n/d	
13	4:1 NH_2	0.06%	n/d	9.8%
14	7:1 NH_2	0.04%	n/d	4.6%

entry	PFAS structure	deF%[a] [# of C-F bonds broken per molecule]	Parent compound decay rate (h^{-1})	deF% (10 M NaOH, 90°C, 2 d)
		Influence of C-H bond location		
15	$CF_3CFHCOOH$	8 h 16.20% [3.82/4F]	0.04±0.01	50.6%
16	$HOOC{-}CF_2{-}CH_2{-}COOH$	38.91±0.31% [1.92±0.63/2F]	0.07±0.01	84.5%
17	$HC_6F_{12}COOH$	0%	-	12.0%
18	$CF_3CHFCF_2CH_2OH$	22.15±2.8% [1.32±0.17/6F]	n/d	-
19	$(CF_3)_2CHCH_2COOH$	109% [6.54/6F]	0.27±0.04	91.4%
20	$CH_3CH_2CF_2{-}COOH$	0.42%	-	1.1%
21	CF_3CF_2COOH	0	-	-
22	$CH_3CHFCOOH$	0.21%	-	-
23	HCF_2COOH	0%	-	82.1%
24	6:2 COOH	0%	-	0.1%
25	6:2 SO_3H	0%	-	0.6%
		Influence double bond		
26	$CF_3{-}CH{=}CH{-}CH_2{-}OH$	0.50%	n/d	-
27	$CF_3{-}CH{=}CH{-}COOH$	12 h 1.57±0.05%	−0.01±0.00	-
28	$C_3F_7{-}CH{=}CH{-}COOH$	0.07±0.03%	0.01±0.00	20.3%
29	$CF_3{-}CF_2{-}CF{=}CF{-}COOH$	35.71% @ 12 h [6.44±2.2/7F]	0.10±0.03	21.6%
30	$C_5F_{11}{-}CF{=}CH{-}COOH$	19.75% [2.37/12F]	1.75±0.58	-
32	$CF_2{=}CF{-}CH_2{-}CH_2{-}COOH$	3.89% @ 12 h [0.58/3F]	0.03±0.051	-
		2,4-Dione		
33	$4FdioneCH_3$	0.06%	n/d	-
34	$4FdioneCF_3$	0.12%	n/d	-

[a]Unless specified otherwise, the reaction conditions are pH 12.0 and 90°C and the deF% were obtained at the end of the reaction.

4.2.4 <u>Technical notes for remediation practice.</u> In this task, we investigated the non-redox and non-photochemical defluorination of specific H-containing PFAS under alkaline conditions. The strong electronegativity of the F atom increases the acidity of the H atom in the polyfluoroalkyl structures, making it prone to attack by aqueous OH^-, allowing HF elimination and further transformations. Besides, the F atom on double bonds is also subject to defluorination under alkaline conditions. These findings provide deeper insights into PFAS transformation in both natural and engineering systems. It is important to consider that H-containing PFAS released into the environment or generated from the transformation of other PFAS may undergo spontaneous defluorination under alkaline conditions. It is highly worth noting that PFAS stock solutions and reaction samples of H-containing PFAS might be unstable under alkaline conditions. For such chemicals (we have provided a large variety of examples in Table 4), the common practice of using

excess NaOH to help dissolve/stabilize acid-type PFAS should be used with caution.

4.3 Further optimization of energy efficiency

In this task, we further optimized the energy consumption by varying the number of UV lamps for PFAS defluorination. While one could readily anticipate that more UV lamps would accelerate defluorination, it remained unclear whether additional UV lamps could proportionally increase the reaction rate (thus, the total electrical energy consumption is consistent) or achieve a higher deF% by triggering additional degradation pathways. Because most electrical energy for the UV lamp is eventually dissipated as heat, the water temperature will gradually rise until it reaches equilibrium, where heat generation balances with dissipation. Increasing the number of UV lamps would heat the water faster and achieve a higher temperature. The optimal temperature for UV/sulfite treatment was determined to be 50°C in the first research task. The remaining question is whether gradual heating by UV lamps could achieve the same PFAS degradation efficacy as preheating the water before turning on UV irradiation. To answer the above questions, we conducted PFAS degradation experiments using 1, 2, and 4 UV lamps. We compared the UV treatment starting from 20°C versus the optimized 50°C regarding PFAS defluorination and energy consumption.

4.3.1 Effects of UV lamp numbers at 50°C. Different numbers of 10 W UV lamps heated the 2 L of water (in the beaker wrapped with aluminum foil) to different temperatures (Table 5). Specifically, two UV lamps kept the water temperature around 50°C. If the water was preheated to 50°C and then the two UV lamps were turned on, the water temperature could be maintained without external heat. Starting at 50°C, the defluorination of PFOA and PFBS by one, two, or four UV lamps did not show a significant difference (Figures 17a and b).

Table 5. Water Heating by UV Lamps.[a]

Number of UV lamps	Temperature of water (2 L)			
	Start @ 20 °C		Start @ 50 °C	
	@ 4h	@ 8h	@ 4h	@ 8h
1	36 °C	36 °C	50 °C	50 °C
2	48 °C	53 °C	53 °C	53 °C
4	65 °C	73 °C	73 °C	73 °C

[a]When one 10 W UV lamp was used, a heating plate was needed to achieve the water temperature at 50°C. With two and four UV lamps, a heating plate was not used after the lamps were turned on.

4.3.2 Effects of UV lamp numbers starting at 20°C. When the photochemical reaction started at room temperature (20°C) and the water was gradually heated by the UV lamps, the use of more UV lamps resulted in faster defluorination (Figures 17c and d). Since the use of just one UV lamp has been sufficient to achieve the maximum deF%, the accelerated defluorination by using additional UV lamps is attributed to the faster temperature increase. For PFOA, the use of one or multiple UV lamps achieved the same deF% (Figure 17c). However, for PFBS, only using one lamp resulted in a lower deF% (Figure 17d) because one UV lamp could merely elevate the water temperature to 36°C in our experimental setting (Table 5). This trend is consistent with our earlier observations with controlled temperature (Figure 5f). That experiment has suggested that the optimal temperature of 50°C allows the cleavage of certain challenging C–F bonds in PFBS and its TPs.

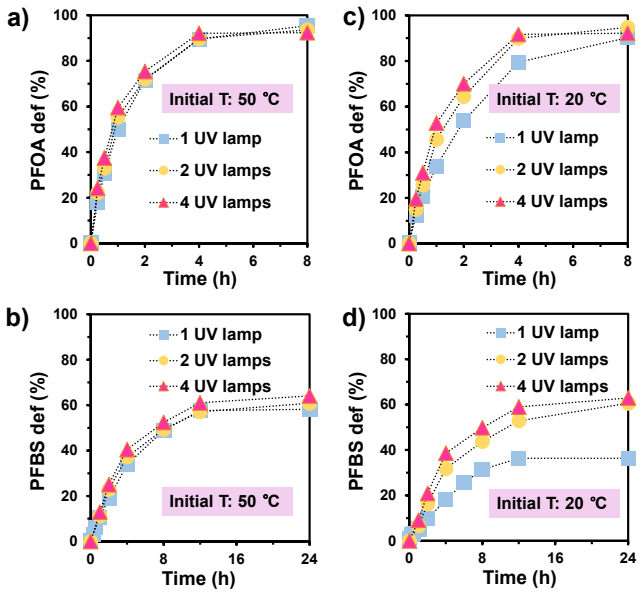

Figure 17. Time profiles for PFOA and PFBS defluorination at the initial temperature of (a and b) 50 °C and (c and d) 20 °C. Reaction conditions: individual PFAS (25 μM), Na_2SO_3 (10 mM), $NaHCO_3$ (5 mM), pH 12.0, and 254 nm irradiation (10 W low-pressure Hg lamps for 2 L solution). No cooling water was used.

4.3.3 Is preheating to 50°C necessary? When two or four UV lamps were used for PFOA and PFBS degradation, preheating the water to 50°C led to slightly faster defluorination than those without preheating (i.e., starting the UV degradation at 20°C but without cooling water). But this difference did not affect the final deF% (Figure 18). Therefore, as long as the final temperature could reach the optimal 50°C, preheating the water could accelerate the initial reaction kinetics but did not impact the total number of C–F bonds to be cleaved.

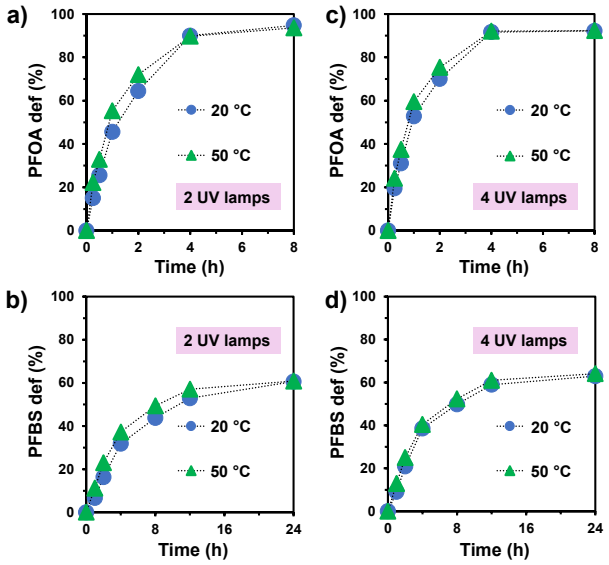

Figure 18. Profiles for PFOA and PFBS defluorination at initial temperatures of 20 °C and 50 °C with (a and b) two or (c and d) four lamps. Reaction conditions: see Figure 17 and Table 5.

4.3.4 ***Comparison of energy consumption.*** Regarding electrical energy consumption, using two UV lamps appeared to be optimal for the specific reactor setting in this project (Table 6). Without extra heating equipment, the heat from two UV lamps was sufficient to raise the water temperature to the optimal 50°C (Table 5) to ensure maximum defluorination (Figure 17). Using four UV lamps, whether preheated to 50°C or not, only enhanced the initial defluorination rate (Figure 17). The time required to reach the maximum deF% was roughly the same as using two UV lamps. If just one UV lamp is available, in order to achieve maximum deF%, preheating the water to 50°C and maintaining the temperature was necessary (Figure 17b versus d). Notably, the corresponding total energy consumption might exceed that of using two UV lamps. In Table 6, for PFOA, 40 kWh/m^3 will be consumed by two lamps, while 54.2 kWh/m^3 will be consumed by one lamp plus preheating. However, we must point out that heat insulation could partially reduce electricity consumption if one lamp and preheating are used. This aspect goes beyond this project because the pilot scale reactor could have various configurations, and the insulation design and temperature control could be largely different.

Table 6. Energy Consumption to Achieve Maximum PFAS Defluorination with Varying Numbers of UV Lamps.[a]

Number of UV lamps	Energy consumption to achieve maximum defluorination (kJ for 2 L and kWh/m^3)			
	Start @ 20 °C[b]		Start @ 50 °C[c]	
	PFOA	PFBS	PFOA	PFBS
1	144 (20)	432 (60)	390 (54.2)[d]	678 (94.2)[d]
2	288 (40)	864 (120)	534 (74.2)	1110 (154.2)
4	576 (80)	1728 (240)	822(114.2)	1974 (274.2)

[a]Reaction conditions: PFAS (25 μM), Na_2SO_3 (10 mM), $NaHCO_3$ (5 mM), pH 12.0, and 254 nm irradiation (10 W low-pressure Hg lamp for 2 L solution).
[b]The energy consumption is calculated as n×t×36, where n represents the number of UV lamps, t denotes the time required to reach maximum defluorination (h), and 36 represents the energy consumption per hour by a 10 W UV lamp (kJ).
[c]The energy consumption is calculated as 245.5+n×t×36, where 245.5 represents the energy consumption for heating 2 L of water from 20℃ to 50 ℃ (kJ).
[d]Estimating the energy consumption required to maintain the temperature at 50°C is not straightforward and not included here. This value could greatly vary by thermal insulation settings, which was not studied by this project except for aluminum foil wrapping outside the reactor.

4.3.5 ***Technical Notes.*** The overlooked heat from UV lamps could greatly aid in PFAS defluorination. For the 2 L reactor used in this study, two 10 W UV lamps proved to be the most efficient configuration. For larger reactor designs, temperature control is very important to ensure the water temperature is within the range for optimal defluorination performance. The cooling water setting for academic research (toward a good temperature control at the commonly adopted 20°C across literature) should not be used for practical applications. Instead, thermal insulation should be applied to the reactor parts to preserve the unavoidable heat from UV lamps. In addition, extra heating equipment might be necessary, depending on the number of UV lamps to be used. The detailed parameters must be determined for the real reactor. The good thing is that the number of UV lamps, the inclusion of heating equipment, and temperature monitoring are all easy engineering designs and can be very flexible.

5. Conclusions and Future Efforts

This project systematically investigated (1) the effect of temperature on PFAS degradation under UV/sulfite treatment; (2) the structure-reactivity relationship and mechanisms for non-photochemical, non-redox defluorination of PFAS at elevated temperature and alkaline conditions; and (3) the overall effect of thermal energy generation and UV irradiation by low-pressure UV lamps on PFAS degradation. Main conclusions include:

(1a) The highest rates of PFAS decay and defluorination are achieved at 50°C. For the three major PFAS structure families (PFCAs, PFSAs, and FTCAs), the decay rates increased by 21–85% when the solution temperature was raised from 20 to 50°C. For the recalcitrant structures that could not be effectively degraded by UV/sulfite treatment (e.g., n=4 PFBS and 4:3 FTCA), the percentage of decay was also improved by 9–19% after 24 h. The defluorination percentage also increased by 3–22% (particularly significant for recalcitrant PFAS structures). The TP analysis suggested that the reaction at 50°C also allowed the cleavage of relatively strong C–F bonds.

(1b) In contrast, further raising the temperature to 90°C resulted in adverse effects. Compared to 20°C, the rates of PFAS decay decreased by 41–66% at 90°C. The percentages of decay and defluorination were similar to those at 20°C, but the rates were slower. Photochemical measurements suggested that the elevated temperature lowered the quantum yield of hydrated electrons. The competition between accelerated elemental reaction steps versus decreased quantum yield of hydrated electrons resulted in the maximum rate for the overall reaction at 50°C. Further increasing the temperature to up to 90°C resulted in a gradual slowing down of the overall reaction.

(1c) The addition of iodide for reaction acceleration also benefited from the elevated temperature to 50°C. However, iodide addition did not alter the PFAS degradation mechanism, so the maximum deF% by UV/sulfite+iodide was the same as by UV/sulfite. The positive effects from both iodide addition and heating to 50°C can synergistically achieve significantly enhanced defluorination performance.

(2) We found a series of H-containing PFAS that allowed non-redox defluorination under alkaline conditions (pH≥9). The 6:2 FTCA ($C_6F_{13}C\mathbf{H_2}COO^-$) showed limited defluorination at pH 9.0 and 20ºC, primarily via HF elimination (i.e., yielding $C_5F_{11}-CF=C\mathbf{H}-COO^-$). Elevated temperature (up to 90ºC) and pH (up to 14) not only accelerated the reaction rate but also intensified the level of defluorination via additional mechanisms, many of which remain elusive. For example, $C_6F_{13}C\mathbf{H_2}COO^-$ could be further transformed into multiple PFCAs $C_nF_{2n+1}-COOH$ (n=4, 3, 2) as the end products. We further extended the PFAS collection to 30+ H-containing PFAS structures and confirmed the general trend that C−H bonds with high acidity are prone to be eliminated alongside neighboring F atoms. The resulting double bonds containing F atoms could be further defluorinated by OH^- attacks. Because of the structure specificity, heating the water at pH 12 after UV/sulfite treatment cannot replace oxidation treatment to achieve 100% defluorination for a majority of PFAS. However, the findings provide important insights into the additional PFAS degradation mechanism under heated alkaline conditions (e.g., UV/sulfite at pH 12 without temperature control) and caution the analytical researchers on sample preservation to avoid gradual defluorination in alkaline solutions.

(3) With the 2 L reactors used in this study, two 10 W UV lamps provided the most cost-effective treatment of both PFOA and PFBS. The thermal energy from UV lamps is sufficient to bring the water temperature to the optimal 50°C, which allows deeper defluorination of the recalcitrant PFBS. Preheating the water to the optimal temperature is not necessary. Overall, the heat dissipated from the UV lamps significantly enhances the rate and extent of PFAS defluorination.

This limited-scope project has confirmed the positive effect of thermal energy, which is the dominant way of electrical energy dissipation from UV lamps (i.e., all energy not utilized for chemical reaction will eventually transform into heat). The findings have been provided to the ESTCP project (ER21-5152) on the treatment of still bottom brines and foam fractionation concentrates. This study did not further test the better-insulated reactors (e.g., using plastic foams or glass wools outside the container rather than aluminum foil) because the pilot- and full-scale systems will have more comprehensive considerations and design guidelines on the heat transfer aspects, such as (1) what part(s) of the system (e.g., reservoir, pipes, and UV module) can be insulated and (2) whether controlled heating and cooling modules are still required from the engineering perspectives. Thus, in this study, we primarily focus on the temperature values and the proof-of-concept rather than developing detailed approaches for heat transfer control. The findings have answered most research questions proposed for this project.

Literature Cited

(1) Song, Z.; Tang, H.; Wang, N.; Zhu, L. Reductive defluorination of perfluorooctanoic acid by hydrated electrons in a sulfite-mediated UV photochemical system. *J. Hazard. Mater.* **2013**, *262*, 332-338. DOI: https://doi.org/10.1016/j.jhazmat.2013.08.059. Cui, J.; Gao, P.; Deng, Y. Destruction of Per- and Polyfluoroalkyl Substances (PFAS) with Advanced Reduction Processes (ARPs): A Critical Review. *Environ. Sci. Technol.* **2020**, *54* (7), 3752-3766. DOI: 10.1021/acs.est.9b05565. Bao, Y.; Huang, J.; Cagnetta, G.; Yu, G. Removal of F–53B as PFOS alternative in chrome plating wastewater by UV/Sulfite reduction. *Water Res.* **2019**, *163*, 114907. DOI: https://doi.org/10.1016/j.watres.2019.114907.

(2) Bentel, M. J.; Yu, Y.; Xu, L.; Li, Z.; Wong, B. M.; Men, Y.; Liu, J. Defluorination of Per- and Polyfluoroalkyl Substances (PFASs) with Hydrated Electrons: Structural Dependence and Implications to PFAS Remediation and Management. *Environmental science & technology* **2019**, *53* (7), 3718-3728. DOI: 10.1021/acs.est.8b06648.

(3) Bentel, M. J.; Yu, Y.; Xu, L.; Kwon, H.; Li, Z.; Wong, B. M.; Men, Y.; Liu, J. Degradation of Perfluoroalkyl Ether Carboxylic Acids with Hydrated Electrons: Structure–Reactivity Relationships and Environmental Implications. *Environmental science & technology* **2020**, *54* (4), 2489-2499. DOI: 10.1021/acs.est.9b05869. Gao, J.; Liu, Z.; Bentel, M. J.; Yu, Y.; Men, Y.; Liu, J. Defluorination of Omega-Hydroperfluorocarboxylates (ω-HPFCAs): Distinct Reactivities from Perfluoro and Fluorotelomeric Carboxylates. *Environ. Sci. Technol.* **2021**, *55* (20), 14146-14155. DOI: 10.1021/acs.est.1c04429.

(4) Bentel, M. J.; Liu, Z.; Yu, Y.; Gao, J.; Men, Y.; Liu, J. Enhanced Degradation of Perfluorocarboxylic Acids (PFCAs) by UV/Sulfite Treatment: Reaction Mechanisms and System Efficiencies at pH 12. *Environmental Science & Technology Letters* **2020**, *7* (5), 351-357. DOI: 10.1021/acs.estlett.0c00236.

(5) Liu, Z.; Bentel, M. J.; Yu, Y.; Ren, C.; Gao, J.; Pulikkal, V. F.; Sun, M.; Men, Y.; Liu, J. Near-Quantitative Defluorination of Perfluorinated and Fluorotelomer Carboxylates and Sulfonates with Integrated Oxidation and Reduction. *Environ. Sci. Technol.* **2021**, *55* (10), 7052-7062. DOI: 10.1021/acs.est.1c00353.

(6) Gao, J.; Liu, Z.; Chen, Z.; Rao, D.; Che, S.; Gu, C.; Men, Y.; Huang, J.; Liu, J. Photochemical degradation pathways and near-complete defluorination of chlorinated polyfluoroalkyl substances. *Nature Water* **2023**, *1* (4), 381-390. DOI: 10.1038/s44221-023-00046-z.

(7) Wu, B.; Hao, S.; Choi, Y.; Higgins, C. P.; Deeb, R.; Strathmann, T. J. Rapid Destruction and Defluorination of Perfluorooctanesulfonate by Alkaline Hydrothermal Reaction. *Environ. Sci. Technol.* **2019**, *6* (10), 630-636. DOI: 10.1021/acs.estlett.9b00506. Hao, S.; Choi, Y.-J.; Wu, B.; Higgins, C. P.; Deeb, R.; Strathmann, T. J. Hydrothermal Alkaline Treatment for Destruction of Per- and Polyfluoroalkyl Substances in Aqueous Film-Forming Foam. *Environmental science & technology* **2021**, *55* (5), 3283-3295. DOI: 10.1021/acs.est.0c06906. Zhang, W.; Cao, H.; Liang, Y. Degradation by hydrothermal liquefaction of fluoroalkylether compounds accumulated in cattails (Typha latifolia). *Journal of Environmental Chemical Engineering* **2021**, *9* (4), 105363. DOI: https://doi.org/10.1016/j.jece.2021.105363. Li, J.; Pinkard, B. R.; Wang, S.; Novosselov, I. V. Review: Hydrothermal treatment of per- and polyfluoroalkyl substances (PFAS). *Chemosphere* **2022**, *307*, 135888. DOI: https://doi.org/10.1016/j.chemosphere.2022.135888.

(8) Bentel, M. J.; Yu, Y.; Xu, L.; Kwon, H.; Li, Z.; Wong, B. M.; Men, Y.; Liu, J. Degradation of perfluoroalkyl ether carboxylic acids with hydrated electrons: Structure–reactivity relationships and environmental implications. *Environ. Sci. Technol.* **2020**, *54*, 2489-2499. Bentel, M. J.; Yu, Y.; Xu, L.; Li, Z.; Wong, B. M.; Men, Y.; Liu, J. Defluorination of per-and polyfluoroalkyl substances (PFASs) with hydrated electrons: structural dependence and implications to PFAS remediation and management. *Environ. Sci. Technol.* **2019**, *53* (7), 3718-3728.

(9) Bentel, M. J.; Liu, Z.; Yu, Y.; Gao, J.; Men, Y.; Liu, J. Enhanced degradation of perfluorocarboxylic acids (PFCAs) by UV/sulfite treatment: Reaction mechanisms and system efficiencies at pH 12. *Environ. Sci. Technol. Lett.* **2020**, *7*, 351-357.

(10) Liu, Z.; Chen, Z.; Gao, J.; Yu, Y.; Men, Y.; Gu, C.; Liu, J. Accelerated Degradation of Perfluorosulfonates and Perfluorocarboxylates by UV/Sulfite + Iodide: Reaction Mechanisms and System Efficiencies. *Environ. Sci. Technol.* **2022**, *56* (6), 3699-3709. DOI: 10.1021/acs.est.1c07608.
(11) Beltran, F. J.; Ovejero, G.; Garcia-Araya, J. F.; Rivas, J. Oxidation of Polynuclear Aromatic Hydrocarbons in Water. 2. UV Radiation and Ozonation in the Presence of UV Radiation. *Industrial & Engineering Chemistry Research* **1995**, *34* (5), 1607-1615. DOI: 10.1021/ie00044a013.
(12) Charbonnet, J. A.; McDonough, C. A.; Xiao, F.; Schwichtenberg, T.; Cao, D.; Kaserzon, S.; Thomas, K. V.; Dewapriya, P.; Place, B. J.; Schymanski, E. L.; et al. Communicating Confidence of Per- and Polyfluoroalkyl Substance Identification via High-Resolution Mass Spectrometry. *Environ Sci Technol Lett* **2022**, *9* (6), 473-481. DOI: 10.1021/acs.estlett.2c00206.
(13) Liu, J.; Wang, N.; Szostek, B.; Buck, R. C.; Panciroli, P. K.; Folsom, P. W.; Sulecki, L. M.; Bellin, C. A. 6-2 Fluorotelomer alcohol aerobic biodegradation in soil and mixed bacterial culture. *Chemosphere* **2010**, *78* (4), 437-444. DOI: https://doi.org/10.1016/j.chemosphere.2009.10.044.
(14) Nabb, D. L.; Szostek, B.; Himmelstein, M. W.; Mawn, M. P.; Gargas, M. L.; Sweeney, L. M.; Stadler, J. C.; Buck, R. C.; Fasano, W. J. In Vitro Metabolism of 8-2 Fluorotelomer Alcohol: Interspecies Comparisons and Metabolic Pathway Refinement. *Toxicological Sciences* **2007**, *100* (2), 333-344. DOI: 10.1093/toxsci/kfm230 %J Toxicological Sciences (acccessed 12/14/2022).
(15) Zucco, C.; Lima, C. F.; Rezende, M. C.; Vianna, J. F.; Nome, F. Mechanistic studies on the basic hydrolysis of 2,2,2-trichloro-1-arylethanones. *The Journal of Organic Chemistry* **1987**, *52* (24), 5356-5359. DOI: 10.1021/jo00233a009.
(16) Shaw, D. M. J.; Munoz, G.; Bottos, E. M.; Duy, S. V.; Sauvé, S.; Liu, J.; Van Hamme, J. D. Degradation and defluorination of 6:2 fluorotelomer sulfonamidoalkyl betaine and 6:2 fluorotelomer sulfonate by Gordonia sp. strain NB4-1Y under sulfur-limiting conditions. *Science of The Total Environment* **2019**, *647*, 690-698. DOI: https://doi.org/10.1016/j.scitotenv.2018.08.012.
(17) Jonathan Clayden, N. G., Stuart Warren. *Organic Chemistry*; Oxford University Press, 2012.
(18) Takeo Komata, K. K. H., Kasukabe; Shinya Akiba, Fujimino. Process for producing 3,3,3-trifluoropropionic acid. 2011.
(19) Siegemund, G.; Schwertfeger, W.; Feiring, A.; Smart, B.; Behr, F.; Vogel, H.; McKusick, B. Fluorine Compounds, Organic. In *Ullmann's Encyclopedia of Industrial Chemistry*.
(20) Chauvin, A.-S.; Gumy, F.; Matsubayashi, I.; Hasegawa, Y.; Bünzli, J.-C. G. Fluorinated β-Diketones for the Extraction of Lanthanide Ions: Photophysical Properties and Hydration Numbers of Their EuIII Complexes. **2006**, *2006* (2), 473-480. DOI: https://doi.org/10.1002/ejic.200500849.

Appendix A. Supplemental Information

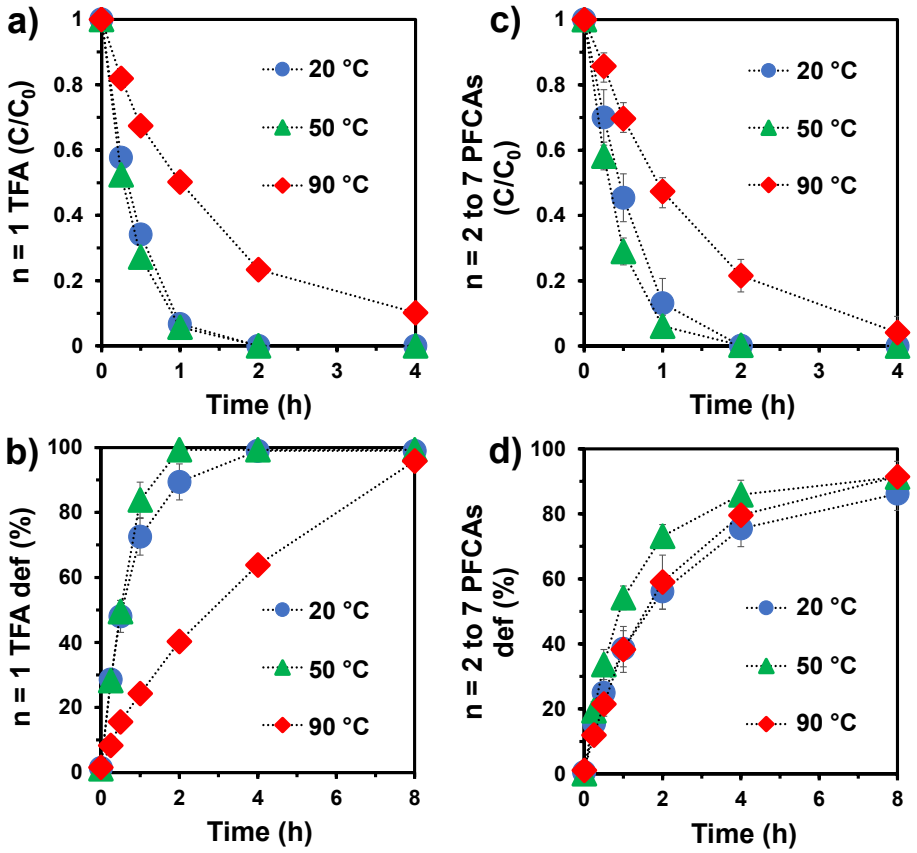

Figure A1. Profiles for (a and c) parent compound decay and (b and d) defluorination of PFCAs at 20, 50, and 90°C. Reaction conditions: individual PFAS (25 μM), Na_2SO_3 (10 mM), $NaHCO_3$ (5 mM), pH 12.0, and 254 nm irradiation (10 W low-pressure Hg lamp for 2 L solution). Note: n ≥2 structures showed similar profiles, and the averaged data are shown in panels (c) and (d).

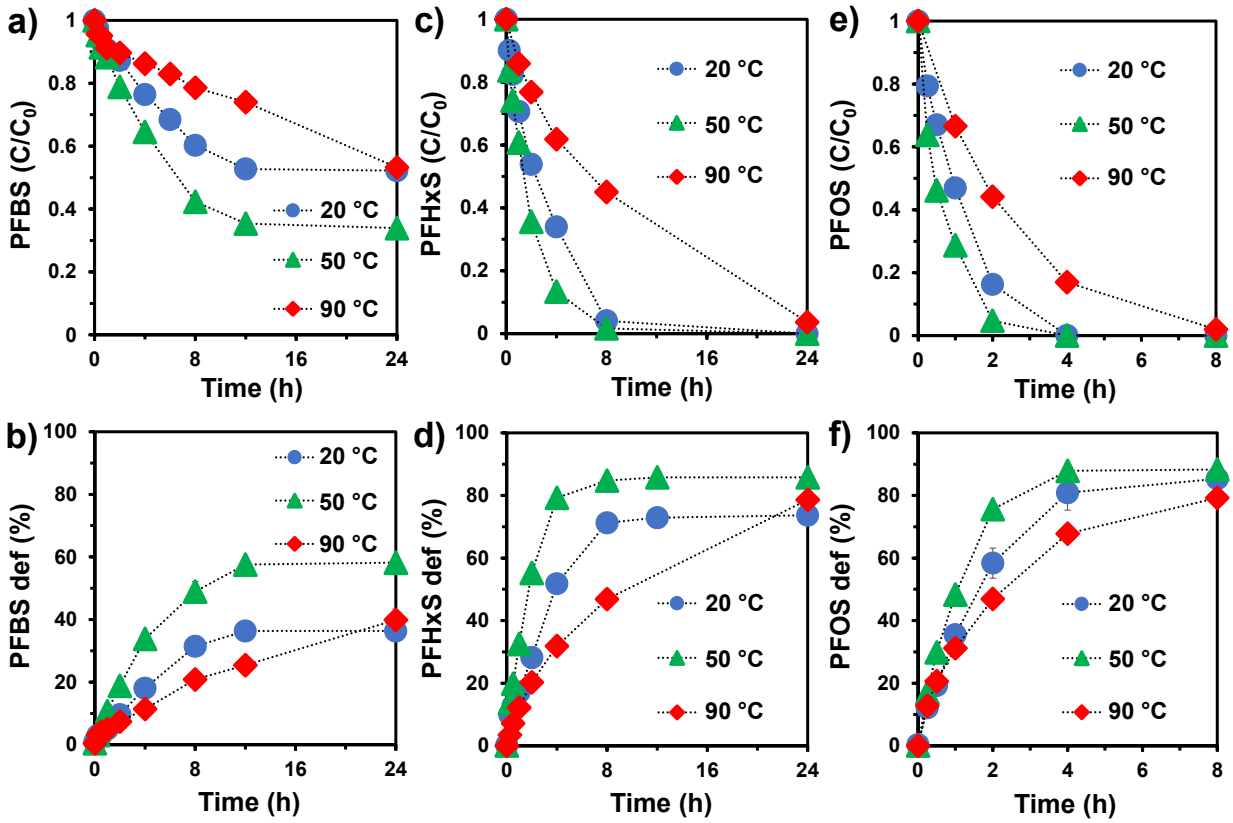

Figure A2. Profiles for (a, c, and e) parent compound decay and (b, d, and f) defluorination of PFSAs at 20, 50, and 90°C. Reaction conditions: individual PFAS (25 μM), Na_2SO_3 (10 mM), $NaHCO_3$ (5 mM), pH 12.0, and 254 nm irradiation (10 W low-pressure Hg lamp for 2 L solution).

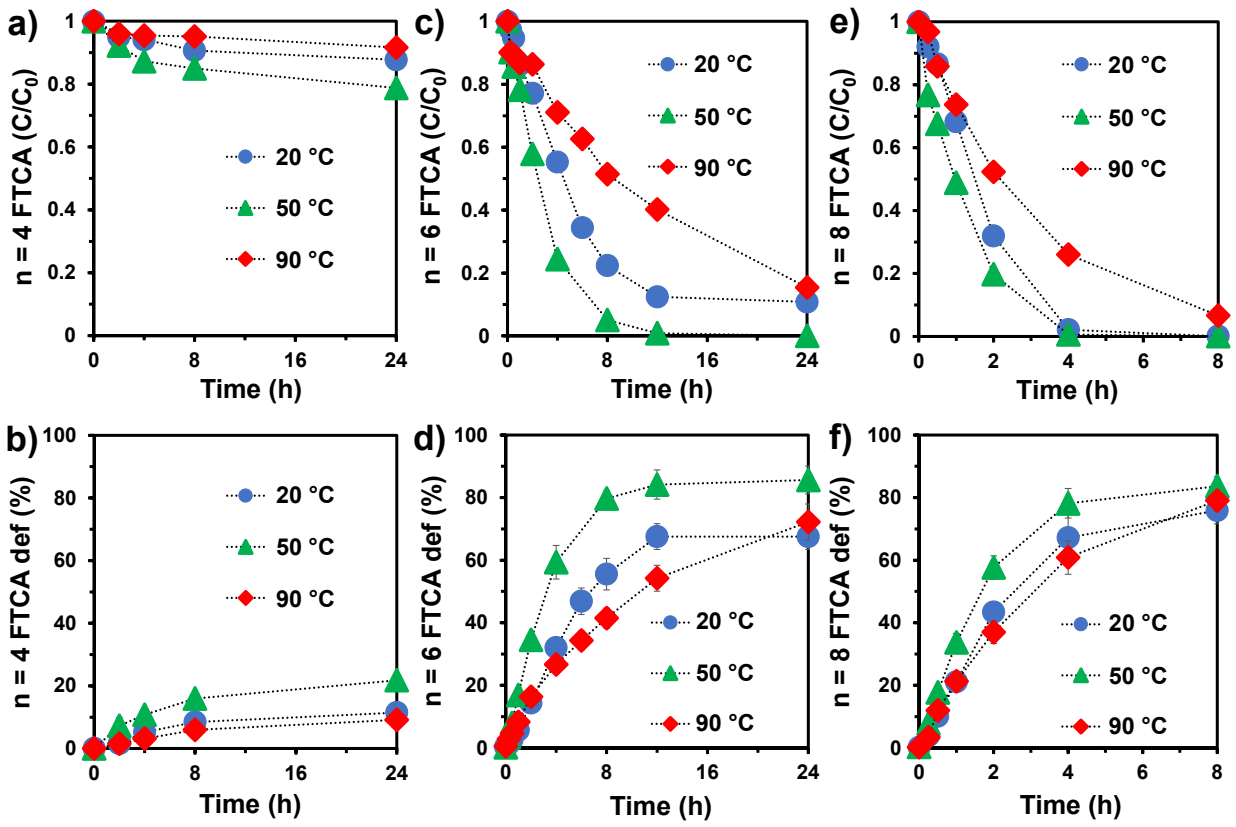

Figure A3. Profiles for (a, c, and e) parent compound decay and (b, d, and f) defluorination of FTCAs at 20, 50, and 90°C. Reaction conditions: individual PFAS (25 μM), Na_2SO_3 (10 mM), $NaHCO_3$ (5 mM), pH 12.0, and 254 nm irradiation (10 W low-pressure Hg lamp for 2 L solution).

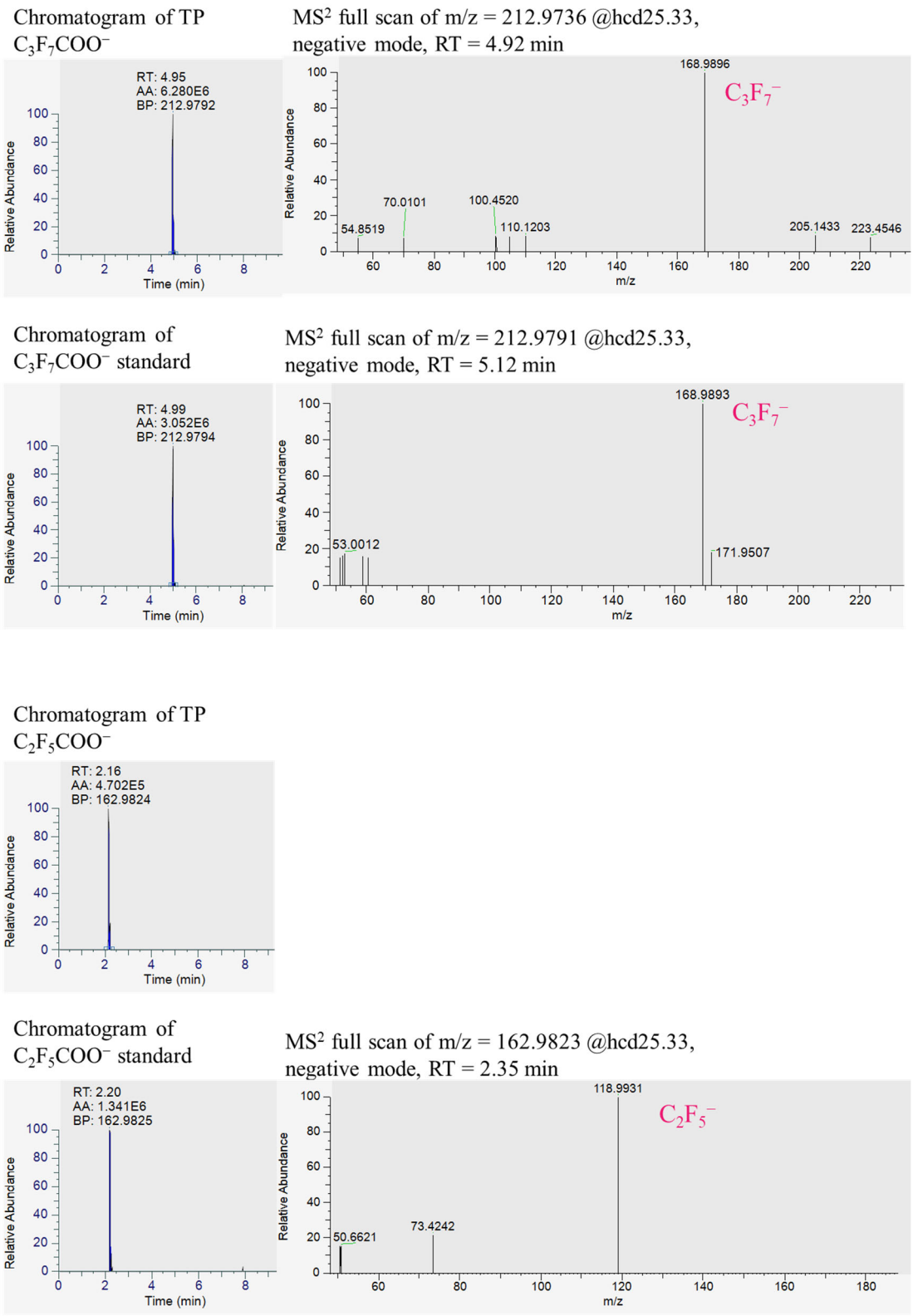

Figure A4. Comparison of the chromatograms and MS^2 fragments of transformation products from 6:2 FTCA with corresponding standard chemical. Conditions: $[6:2\ FTCA]_{ini}$ = 250 μM, 90°C, pH 12.

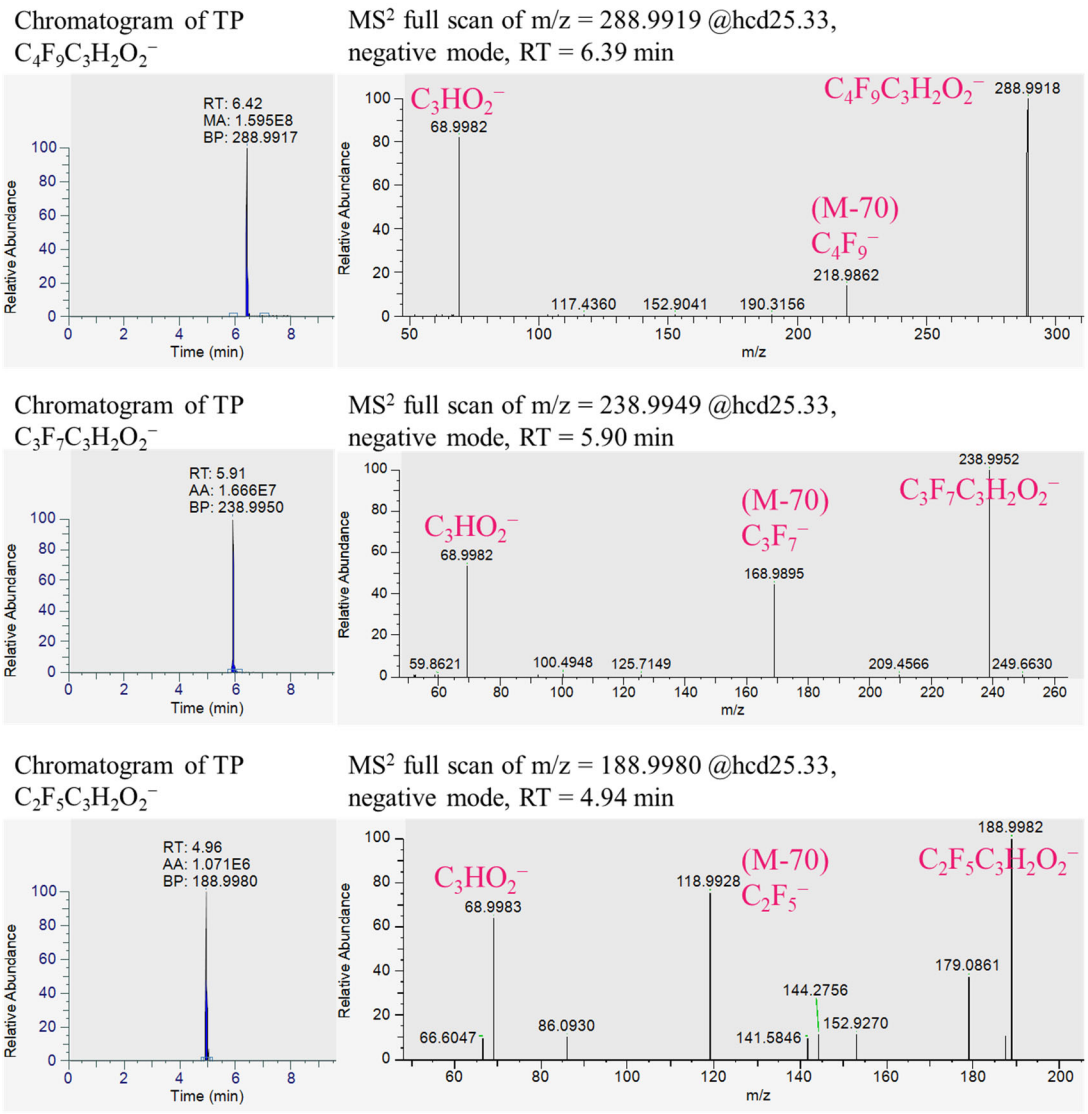

Figure A5. Chromatogram and MS^2 fragments of the transformation products C_nF_{2n+1}–$C_3H_2O_2^-$ (n=4, 3, 2) from 6:2 FTCA. Conditions: $[6:2\ FTCA]_{ini}$ = 250 μM, 90ºC, pH 12. The data were collected from the sample collected after the reaction for 2 h.

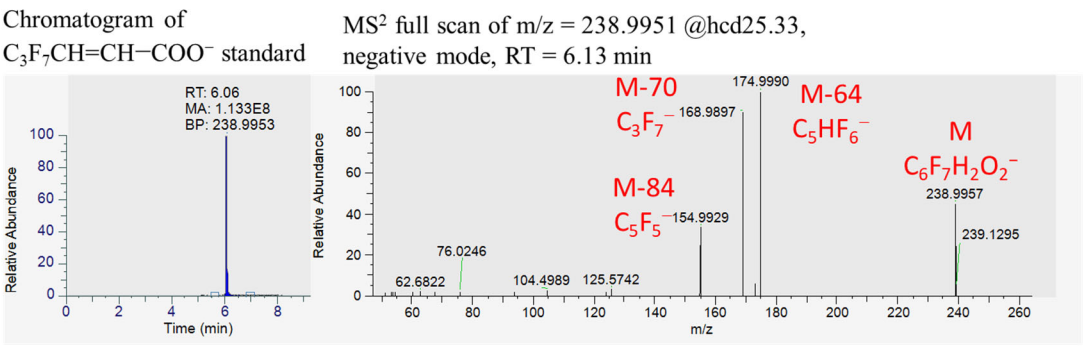

Figure A6. Chromatogram and MS^2 fragments of $C_3F_7CH{=}CH{-}COO^-$ standard.

Text A1. Determination of the photon flux (I_0) and the effective path (L) of radiation of the photolysis reactor

According to Lambert-beer's law, the disappearance rate of an actinometer substance (a) is given by:

$$-\frac{dC_a}{dt} = \Phi_a I_0 (1 - e^{-2.303 L \varepsilon_a C_a}) \quad \text{(S1)}$$

Here, Φ_a, ε_a, and C_a represent the quantum yield, extinction coefficient, and concentration of the actinometer, respectively. Eq. S1 can be simplified into two scenarios based on the value of the exponential term:

If $2.303 L \varepsilon_a C_a > 2$,

$$-\frac{dC_a}{dt} = \Phi_a I_s \quad \text{(S2)}$$

If $2.303 L \varepsilon_a C_a < 0.2$,

$$-\frac{dC_a}{dt} = 2.303 L \Phi_a I_s \varepsilon_a C_a \quad \text{(S3)}$$

With a known Φ_a, Eq. S2 can be used to determine I_0, followed by applying Eq. S3 for determining L.

(a) Determination of I_0:[11]

A 0.062 M H_2O_2 solution served as the chemical actinometer for measuring I_0. Initially, the high-concentration H_2O_2 satisfied the condition $2.303 L \varepsilon_a C_a > 2$, leading to the equation:

$$-\frac{d[H_2O_2]}{dt} = \Phi_{H_2O_2} I_0 \quad \text{(S4)}$$

It is reported that $\Phi_{H_2O_2} = 1.0$. By monitoring the concentration of H_2O_2 using the ABTS colorimetric method at pH 2.0,[4] we observed the decay rate of H_2O_2 during the photolysis reaction to be 2.9×10^{-6} s^{-1} (Figure A7). Applying Eq. S4, we calculated the I_0 value as 2.9×10^{-6} einstein $cm^{-2}s^{-1}$.

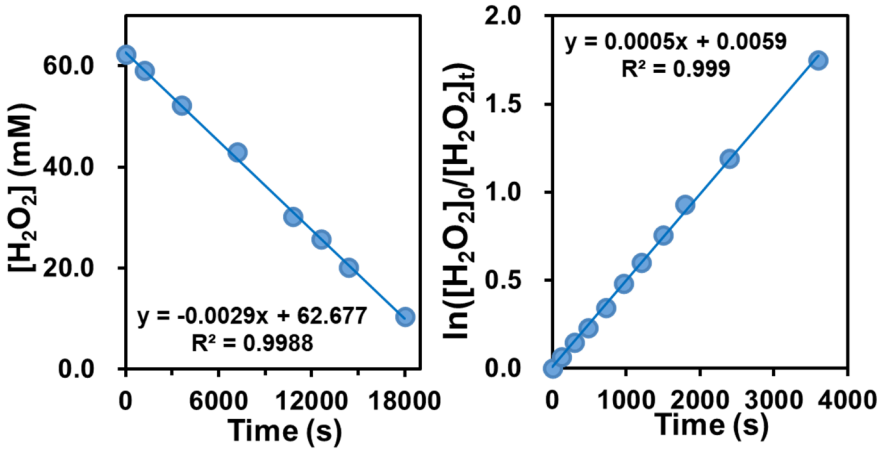

Figure A7. Decay kinetics of 62 mM H_2O_2 (left) and 100 μM H_2O_2 (right) in the photolysis reactor used in this study.

(b) Determination of L:[11]

The average light path length (L) of the reactor was determined using 100 μM H_2O_2 as the chemical actinometer. In this case, Eq. S3 was used, and $I_0 = 2.9\times10^{-6}$ einstein $cm^{-2}s^{-1}$, $\varepsilon_{H_2O_2}$=19 $M^{-1}\cdot cm^{-1}$, $\Phi_{H_2O_2}$(total quantum yield) = 1.0 $mol\cdot einstein^{-1}$. Eq. S3 indicates first-order decay kinetics for H_2O_2, so a linear plot of $\ln(C/C_0)$ vs. time was drawn (Figure A7), and the slope of this plot equals $2.303L\Phi_a I_0 \varepsilon_a$. From the available data, L was calculated to be 3.9 cm.

Text A2. Energy consumption for heating the water and UV

The isochoric heat capacity values for water at various temperatures are presented in the Table below. Energy consumption for heating 2 liters (approximately 2 kg) of water from 20℃ to 50℃ was determined through trapezoidal integration.

$$\boldsymbol{Q = \int_{T_1}^{T_2} mC_V(T)\,dT = m\frac{C_V(T_1) + C_V(T_2)}{2}(T_2 - T_1) = 245.5\ kJ}$$

When a 10-W UV lamp is used to irradiate 2 L of water, the electrical energy consumption per hour totals 36 kJ. Consequently, the energy required to heat the water to 50℃ is equivalent to the energy utilized in UV-sulfite treatment for 6.8 h.

Isochoric Heat Capacity of Water

Temperature (℃)	Isochoric Heat Capacity (kJ kg^{-1} K^{-1})
20	4.1570
25	4.1379
30	4.1175
40	4.0737
50	4.0264
60	3.9767
70	3.9252
80	3.8729
90	3.8204
100	3.7682
110	3.7167
120	3.6662

Text A3. Acidity of the $-CH_2-$ Group in nFdioneCH$_3$, nFdioneCF$_3$, and $C_nF_{2n+1}-C(O)-CH_2-CHO$

The acidity of the $-CH_2-$ group in these structures is attributed to the strong electro-withdrawing effect of $C_nF_{2n+1}-$ and the conjugate base resonance stabilization of carbonyl groups.[19] According to the reported p*K*a of $CF_3COCH_2CO\mathbf{C}H_3$ (6.7) and $CF_3COCH_2CO\mathbf{C}F_3$ (4.6),[20] it is expected the p*K*a of $CF_3-C(O)-CH_2-C\mathbf{H}O$ should be in the range of 4.6−6.7. For longer chain $C_nF_{2n+1}-C(O)-CH_2-C\mathbf{H}O$ (i.e., n >1), the electronegativity of $C_nF_{2n+1}^-$ part will be higher than CF_3-, which will lead to a further decrease of the p*K*a of $C_nF_{2n+1}-C(O)-CH_2-C\mathbf{H}O$. Therefore, it is reasonable that $C_nF_{2n+1}-C(O)-CH_2-C\mathbf{H}O$ of various chain lengths would dissociate as acids and be detected using LC−HRMS/MS.